Copy 2 of 4
RM E57F18

the copy no. on this sheet was changed as copy 2 was destroyed in error.

NACA

RESEARCH MEMORANDUM

A THEORETICAL AND EXPERIMENTAL STUDY OF BORIC OXIDE DEPOSITION ON A SURFACE IMMERSED IN AN EXHAUST GAS STREAM FROM A JET-ENGINE COMBUSTOR, INCLUDING A METHOD OF CALCULATING DEPOSITION RATES ON SURFACES

By Paul C. Setze

Lewis Flight Propulsion Laboratory
Cleveland, Ohio

NATIONAL ADVISORY COMMITTEE
FOR AERONAUTICS

WASHINGTON

October 8, 1957

NATIONAL ADVISORY COMMITTEE FOR AERONAUTICS

RESEARCH MEMORANDUM

A THEORETICAL AND EXPERIMENTAL STUDY OF BORIC OXIDE DEPOSITON ON A SURFACE IMMERSED IN AN EXHAUST GAS STREAM FROM A JET-ENGINE COMBUSTOR, INCLUDING A METHOD OF CALCULATING DEPOSITION RATES ON SURFACES

By Paul C. Setze

SUMMARY

The deposition rate of boric oxide from a stream containing submicron particles was found experimentally to fit a molecular diffusion equation as follows:

Particle diffusion rate (particles/(sq ft)(sec))
= 18.08 (velocity of particles treated as ideal gas molecules (ft/sec))
times (particle volume concentration in free stream (particles/cu ft))

The particle-velocity expression, taken from the kinetic theory of gases, assumes that the particle acts like a molecule of an ideal gas of molecular weight equal to the product of the particle mass times Avogadro's number. The particle volume concentration is calculated from knowledge of the fuel, fuel-air ratio, temperature, and pressure.

This equation enables the calculation of boric-oxide deposition rates to within ±15 percent on surfaces where conventional flow patterns exist. The assumptions and conditions limiting the use of the equation are discussed. The range of the experimental program covered typical turbojet primary-combustor operating conditions.

A discussion of the effect of boric oxide deposits on jet engine performance is included.

INTRODUCTION

The deposition of boric oxide B_2O_3 on surfaces in the turbine region of jet engines operating on boron-containing fuels results in engine-performance deterioration (refs. 1 and 2). A better understanding of the

mechanism of boric oxide deposition in this region could result in reduction of these losses, and thus would hasten the time when boron hydrides would be used operationally as fuels for turbojet engines. For this reason, an investigation of the deposition characteristics of boric oxide was performed at the NACA Lewis laboratory.

Reference 3 suggests that the first step in solving this problem is the determination of growth rates of liquid-boric oxide particles. Data on these growth rates are presented in reference 4. The particle diameter for residence times and conditions existing in typical turbojet engine primary combustors was found to be between 1.0×10^{-5} and 1.5×10^{-5} centimeters. It was also suggested in reference 4 that boric oxide deposition is a diffusional process because of the extremely small particle sizes. By using this theory as a starting point, the original analysis was modified; and a theoretical equation, expressing deposition rate as a function of exhaust-gas stream parameters, was derived.

The results of both the theoretical and experimental work are reported herein, along with a discussion of the effect of deposition on engine performance.

This report is divided into three parts. The first (THEORY) gives in detail two possible mechanisms for the deposition of near molecular-size (1000- to 2000-angstrom units) particles on a surface and develops theoretical equations for each. The second part (EXPERIMENTAL APPARATUS AND PROCEDURE, RESULTS AND DATA CORRELATION, AND CALCULATION METHOD) presents the results, shows how the necessary empirical constants were obtained to compare properly the results with theory, and applies the results to a method of calculating boric oxide deposition rates on engine surfaces. The third part (DISCUSSION AND APPLICATION OF RESULTS, AND CONCLUDING REMARKS) discusses the applicability of the calculation method and the effect of deposits on engine performance.

An example of the use of the calculation method appears in appendix B.

THEORY

General Discussion of Problem

The theoretical analysis is based on the results of the particle-size determinations of reference 4; that is, the particles are small enough to assume that their motion is essentially molecular. From this assumption, a net particle flux from regions of relatively high concentration to regions of low concentration might occur by two processes: molecular diffusion, turbulent diffusion, or a combination of both. (Diffusion caused by Brownian motion also might be considered, but it is negligible for the conditions of interest.)

In general, when a stream is turbulent, diffusion processes occur within the boundaries of the stream at a much faster rate than that predicted by molecular diffusion considerations. However, the present discussion involves particles which are small enough that their motion is essentially molecular, but which are quite large when compared with typical gas molecules such as oxygen or nitrogen. If the scale of turbulence in the stream approached the diameter of the particles, an expression describing the deposition of these particles on surfaces might be expected to contain terms corresponding to both molecular and turbulent diffusion. Therefore, the two diffusion mechanisms will be treated separately, and the experimental data will be used to determine which one, or combination, actually is controlling the deposition process.

Turbulent Diffusion

In order to obtain a turbulent diffusion rate, the well-known Reynold's analogy for the relation between the transfer of momentum and the transfer of mass in a boundary layer on a surface will be used. This relation can be stated as follows:

$$\frac{\text{Rate at which mass is transferred to surface}}{\text{Rate at which mass flows in free stream}}$$

$$= \frac{\text{Rate of momentum loss in boundary layer due to friction}}{\text{Total momentum of free stream flowing over surface}}$$

which can be written

$$\frac{N_T}{n_0 \overline{U}_0} = \frac{g\tau_w}{\rho_0 U_0^2} \tag{1}$$

(A list of the symbols used in this report is given in appendix A.) In equation (1), the only factors that are not immediately obtained from a knowledge of free-stream conditions are the turbulent diffusion rate N_T and the shear stress at the surface τ_w.

Reference 5 gives an expression for τ_w, provided that the shape of the velocity profile in the boundary layer is assumed. A good approximation in most applications is to assume that

$$u = U_0(y/\delta)^{1/7} = U_0\eta^{1/7} \tag{2}$$

where

$$\eta = (y/\delta) \tag{3}$$

By using equation (2) and the definition of τ_w in reference 5, it can be shown that

$$\tau_w = \frac{\rho_0 U_0^2}{g} \frac{\partial \delta}{\partial x} \int_0^1 (1 - \eta^{1/7})\eta^{1/7} \, d\eta = \frac{7}{72} \frac{\rho_0 U_0^2}{g} \frac{\partial \delta}{\partial x} \tag{4}$$

Normally, the boundary-layer thickness can be expressed as follows:

$$\delta = k \frac{x}{Re^a} = k\left(\frac{\nu}{U_0}\right)^a x^{1-a} \tag{5}$$

Then

$$\frac{\partial \delta}{\partial x} = k(1-a)\left(\frac{\nu}{U_0}\right)^a x^{-a} = \frac{k(1-a)}{Re^a} \tag{6}$$

Substitution of equation (6) into equation (4) gives

$$\tau_w = \frac{7}{72} \frac{\rho_0 U_0^2}{g} \frac{k(1-a)}{Re^a} \tag{7}$$

Substitution of equation (7) into equation (1) gives an expression for the turbulent diffusion rate N_T in terms of known stream parameters:

$$N_T = 0.09722 \, n_0 U_0 k \frac{(1-a)}{Re^a} \tag{8}$$

Molecular Diffusion

Loeb (ref. 6) shows that the flux of molecules N passing through a unit area in unit time can be expressed by

$$N = \frac{1}{3} \xi n \tag{9}$$

Now, if one mean free path away l (in the y direction) the concentration is $n - l\left(\frac{dn}{dy}\right)$, the net flux in the y direction is

$$N_{net} = \frac{1}{3} \xi n - \frac{1}{3}[n - l(dn/dy)] \tag{10}$$

which reduces to

$$N_{net} = \frac{1}{3} \xi l \frac{dn}{dy} = N_m \tag{11}$$

or, by defining the diffusion coefficient D as

$$D = \frac{1}{3} \xi l \tag{12}$$

then

$$N_m = D \frac{dn}{dy} \tag{13}$$

which expresses the molecular diffusion rate in terms of a known diffusion coefficient and a concentration gradient.

Discussion of Theoretical Equations

Generally, the diffusion of a molecular species to or from a turbulent stream is governed by the turbulent diffusion rate. However, in the application discussed in this report, the liquid particles, although assumed to be governed by the laws of molecular motion, are rather large as compared with normal molecular sizes. The scale of turbulence decreases rapidly near a surface; therefore, the scale of turbulence might approach the particle size as the surface is approached. This could mean that, while turbulent diffusion might aid in bringing the particle near the surface, molecular diffusion actually would be the driving force across a very thin film on the surface, which might be called a laminar sublayer with respect to the particle (see ref. 7). Because of the physical properties of the particles, it is assumed that every particle colliding with the surface remains at the surface. Therefore the particle concentration approaches zero at the wall. Based on this discussion, the particle concentration profile might be illustrated by the following sketch:

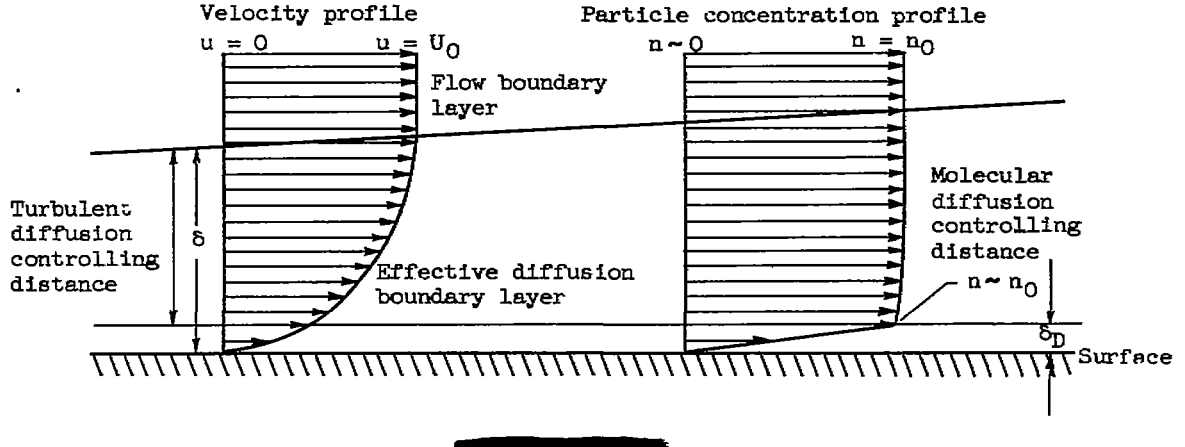

EXPERIMENTAL APPARATUS AND PROCEDURE

General Apparatus

The experimental program consisted of two phases: the first, to determine the boundary-layer characteristics of the test surface; and the second, to determine the deposit characteristics of the test surface. The apparatus used in each phase was the same except for the instrumentation.

A photograph and a schematic diagram of the test apparatus are shown in figure 1. Combustion air from the laboratory central air-supply system entered the apparatus, was measured with an ASME standard orifice, and was throttled through a remotely operated throttle valve. The air then entered the inlet plenum and went through a series of wire and cheese cloth screens that removed dirt and insured a uniform velocity profile. The combustor (just downstream of the inlet plenum) is a standard jet-engine tubular combustor. The fuel injector is air atomizing and is the same as reported in reference 8. From the combustor, the exhaust products entered a calming section where the velocity was about 60 feet per second or less. In this section, any large oxide particles sheared from the combustor walls settled out; thus the diameter of all the particles entering the test section would be between 1.0×10^{-5} and 2.0×10^{-5} centimeters. The test section (fig. 1) consisted of a duct of constant width (4 in.) and varying height (3.70 in. at the inlet and 18.20 in. at the exit). A wedge, 4 inches wide and 12 inches long with upper and lower surfaces parallel to the top and bottom of the test section, was used as the test surface. The wedge was positioned in the foreward part of the test section, and a rectangular spacer filled up the remaining length. The upper surface of the wedge was the test surface. Two ducts carried the gas stream from the test section into the exit plenum, where the gases were quenched with water sprays and were discharged into the building exhaust system.

The fuel systems for pentaborane and JP-4 fuel were the same as reported in reference 9. The fuel system used in the trimethyl borate - methyl alcohol azeotrope (TMB) tests consisted of a 2000-gallon storage tank, a pump, remotely operated throttle and shutoff valves, and provisions for purging the fuel lines. A diagram of the TMB fuel system is shown in figure 2. The fuel flow in each system was measured with a rotating-vane-type flowmeter.

Instrumentation

The following table summarizes the instrumentation that was used in both the boundary-layer and deposition tests:

Station	Station description	Number of temperature points	Number of pressure points
1	Combustor inlet (air)	3	1 (static)
	Combustor inlet (fuel)	1	0
2	Combustor exit	7 (av.)	1 (static)
3	Upper, lower (or both) test-section exit ducts	5	1 (static), av. of 5 (total)

During the boundary-layer tests, the test surface was instrumented with surface thermocouples and surface static-pressure taps (12 of each) placed 1 inch apart along the test surface.

Boundary-Layer Test Procedure

The boundary-layer thickness and velocity profile were measured with a total-pressure probe. The details of the probe are shown in figures 3 and 4. The pressure impulse was converted to a voltage by a pressure transducer, and the output was recorded on two instruments: (1) the Y-axis of an X-Y self-balancing recording potentiometer, which made visual monitoring of the boundary-layer profile possible while a run was in progress, and (2) a high-speed, self-balancing recording potentiometer that was used because of its greater accuracy. The probe was moved by a remotely operated actuator equipped with a variable precision resistor that indicated the probe position. The output from the resistor was recorded on the X-axis of the X-Y recorder.

When the probe, electrically insulated from the rest of the apparatus, touched the test surface, it closed a circuit that actuated the pen on the X-Y recorder, which in turn indicated the position of the test surface in relation to the actuator travel. The total actuator travel was 1/2 inch, and the accuracy of the position indicator was $\pm$0.003 inch. The pressure transducer and the position indicator were calibrated before and after each test.

Deposition Test Procedure

In making the deposition tests, inlet airflow and temperature were established, and the combustor was ignited on JP-4 fuel. The combustor outlet temperature was adjusted to the test conditions. When temperature equilibrium on the test surface was reached, either the TMB or pentaborane fuel flow was initiated, and the test fuel flow was adjusted. When the test fuel had entered the combustor, the JP-4 fuel was turned off, and the conditions were held constant for some predetermined time at which the run was terminated.

The upper wedge surface (test surface) was washed to remove the boric oxide deposit, and the resultant boric acid solution was chemically analyzed for the total quantity of boric oxide. A mean value of the deposition was taken because, after a very short running time, some flow of the oxide occurred along the surface and made accurate determinations of local deposition rates impossible. In tests where oxide was blown back into the separation zone (discussed in a later section), the wedge and the separated surfaces were analyzed separately.

The residence time was calculated by using flow-continuity relationships and the dimensions of sections between the combustor and the test section. From the residence time, a particle size in the test section was calculated by using the method of reference 4.

Preliminary Tests

Several preliminary tests were conducted in order to determine the test-section velocity and temperature profiles, the temperature drop between the test section and the exit ducts, and the time required for the test section to come to temperature equilibrium. The results of these tests showed that about 8 minutes of warm-up time was required. The local velocity across the test section varied less than 3 percent from the average for the range investigated. Typical test-section temperature profiles are shown in figure 5.

RESULTS AND DATA CORRELATION

Boundary-Layer Studies

Fifty-nine boundary-layer thickness measurements were made over the following range of conditions:

Free-stream velocity, ft/sec	44 to 1983
Temperature, $^{\circ}R$	498 to 1618
Reynolds number (xU_0/ν_0)	1.50×10^5 to 4.71×10^6

The coordinate system used in the boundary-layer studies is illustrated in figure 6.

The results are presented in table I and figure 7. A line was fitted to the data, which resulted in the following equation:

$$\frac{\delta}{x} = 0.139(Re)^{-0.22} \qquad (14)$$

From the boundary-layer data, the probable error of any data point referenced to equation (14) was calculated to be ±5.58 percent. As seen in figure 7, the data fall somewhat below the classical flat-plate line. This result was not unexpected, since reference 7 shows this trend for surfaces with a slightly positive pressure gradient (as on a wedge).

Deposition Studies

Eighteen deposition tests were made, thirteen with TMB and five with pentaborane. The data are summarized in table II. Photographs of the wedge and test section after typical trimethyl borate (run 9) and pentaborane (run 15) tests are shown in figure 8. As seen in figure 8(a), the deposit on the wedge surface was quite uniform up to the point where the wedge met the spacer block. Flow separation occurred at the point where the wedge and spacer block met and resulted in two effects: (1) in the region of flow separation, the deposition rate was greatly reduced; and (2) boric oxide, pushed from the wedge into the separated region, remained there and continued to build up (fig. 8b).

The first step in the data correlation was the introduction of the constants a and k from the experimental boundary-layer data into equation (8) (turbulent diffusion equation), which gives:

$$\frac{N_T}{n_0} = 0.0105 \frac{U_0}{Re^{0.22}} \tag{15}$$

If turbulent diffusion is the controlling mechanism, a plot of (N_{tot}/n_0) against $(U_0/Re^{0.22})$ would be expected to result in a straight-line log-log plot, although the slope might be other than unity. This plot was made, and no line could be drawn through the data. A second plot of N_{tot} against $(U_0 n_0 (Re^{0.22})$ was made, and the following equation was taken from data (fig. 9):

$$N_{tot} = 5.51 \times 10^6 \left(\frac{U_0 n_0}{Re^{0.22}} \right)^{0.514} \tag{16}$$

This equation indicates that turbulent diffusion is not the controlling mechanism for, if it were, N_{tot} would be directly proportional to n_0. The terms involved in a molecular diffusion process were also examined by determining an effective diffusion coefficient D_{eff} and a distance which this diffusion coefficient was controlling. This distance will be referred to as the diffusion boundary-layer thickness and will be denoted by δ_D. In determining D_{eff} and δ_D, the following assumption was made:

[redacted]

The concentration of particles at $y = \delta_D$ is equal to the free-stream concentration n_0. This assumption, which is valid only in cases where uniform flow (no separation) is present, is justified because the flow of particles through the diffusion boundary layer, rather than the turbulent diffusion through the turbulent boundary layer, will control the total flux to the wall.

If an expression similar to equation (14) is used to describe the diffusion process, an explicit solution for both D_{eff} and δ_D cannot be obtained by using the experimental data available. Therefore an assumption regarding one of the two unknowns must be made, and it was assumed that the diffusion boundary layer is identical in thickness to the mean free path in the binary mixture (ref. 6, p. 99). In other words,

$$\delta_D \equiv l_0 \tag{17}$$

By using this assumption and the experimental data, the effective diffusion coefficient was calculated from the following equation:

$$D_{eff} = \frac{N_{tot} l_0}{n_0} \tag{18}$$

The effective diffusion coefficient was compared with the theoretical molecular diffusion coefficient (using the mean free path of the binary mixture and assuming the particle velocity to be equal to the theoretical molecular velocity) and was found to vary linearly with it, as indicated by the following expression:

$$D_{eff} = 54.23\ D_m \tag{19}$$

which is illustrated in figure 10. The absolute arithmetic average deviation of all the experimental data from equation (19) was ± 12.5 percent. The implication is that molecular diffusion across a thin layer in the boric oxide - air mixture controls the boric oxide deposition rate.

The combination and rearrangement of equations (12), (18), and (19) give the following experimentally determined expression for the diffusion of boric oxide particles to a surface:

$$N_{tot} = 18.08\ \xi_p n_0 \tag{20}$$

CALCULATION METHOD

Derivation

The following discussion illustrates how equation (20) can be used to calculate boric oxide deposition rates. The assumptions used in the derivation of the equations necessary for the solution of the deposition rate will be consistent with the assumptions used in reference 4, which are:

(1) The liquid particle may be treated as a large ideal gas molecule.

(2) The particles are spherical.

(3) The particle concentration is constant across the main flow stream.

(4) The free-stream conditions are such that essentially all of the boric oxide is in the liquid phase.

In order to calculate deposition rates on surfaces, the parameters n_0 and ξ_p must be known. The following discussion shows how the parameters are found and how they can be used to calculate deposition rates.

Loeb (ref. 6) shows that the average velocity of an ideal gas molecule may be expressed by

$$\xi = \sqrt{\frac{8RT}{\pi m}} = 1.597\sqrt{\frac{RT}{m}} \tag{21}$$

For the case of particles acting as ideal gas molecules,

$$m = W_p N_{Av} \tag{22}$$

where

$$W_p = (\rho_{liq})\left(\frac{1}{6}\pi d_p^3\right) \tag{23}$$

Therefore

$$\xi_p = 2.84\times10^{-12}\sqrt{\frac{RT}{\rho_{liq} d_p^3}} \tag{24}$$

Before solving equation (24), d_p must be calculated. Reference 4 shows that

$$d_p = \left(0.2056 \frac{v_{liq}}{v_g} t\sqrt{\frac{RT}{\rho_{liq}}}\right)^{0.4} \times 10^{-4} \tag{25}$$

In this equation, only v_{liq}/v_g (the ratio of liquid volume to gas volume in the system, which is a function of fuel type, φ, P, and T) is unknown.

The number of pound-moles of gas phase per pound of boric oxide X formed during combustion (assuming no dissociation or B_2O_3 vapor), along with the operating temperature, static pressure, and boric oxide liquid density ($\rho_{liq} = f(T)$ only), can be combined to yield v_{liq}/v_g in the following manner: X = f(fuel type, equivalence ratio) only. Let

$$Y = P/\rho_{liq}RT \tag{26}$$

Then

$$\frac{v_{liq}}{v_g} = \frac{Y}{X} \tag{27}$$

which equates (v_{liq}/v_g) to fuel type, φ, T, and P. If v_{liq}/v_g is known, the particle diameter may be found, and then

$$n_0 = \left(\frac{v_{liq}}{v_g}\right)\left(\frac{1}{v_p}\right) = \left(\frac{v_{liq}}{v_g}\right)\left(\frac{6}{\pi d_p^3}\right) \tag{28}$$

which gives all the information necessary for a deposition-rate calculation.

General Method

(Each equation is dimensionally correct and will yield a correct result as long as consistent units are used.) The steps for calculating the deposition rates are as follows:

(1) Start with the fuel type and fuel-air ratio to calculate the equivalence ratio φ:

$$\varphi = \frac{\text{Actual fuel-air ratio}}{\text{Stoichiometric fuel-air ratio}} \tag{29}$$

(2) By knowing the fuel type and Φ, get X from figure 11.

(3) By knowing the temperature and static pressure, get Y from figure 12.

(4) Calculate (v_{liq}/v_g) from

$$(v_{liq}/v_g) = Y/X \text{ (dimensionless)} \tag{27}$$

(5) Find residence time of particles from formation to point where deposition rate is desired using flow continuity relationships and areas of the system.

(6) Calculate particle diameter from

$$d_p = \left(0.2056 \frac{v_{liq}}{v_g} t\sqrt{\frac{RT}{\rho_{liq}}}\right)^{0.4} \times 10^{-4} \tag{25}$$

$\left(R = \frac{\text{dyne-cm}}{(\text{mole})(^{\circ}\text{K})}, T = {}^{\circ}\text{K}; \rho_{liq} = \text{gm/cm}^3; t = \text{sec}; \text{ and } d_p = \text{cm}\right)$

(7) Calculate n_0 from

$$n_0 = \left(\frac{v_{liq}}{v_g}\right)\left(\frac{6}{\pi d_p^3}\right) \tag{28}$$

(8) By knowing T and d_p, calculate ξ_p from

$$\xi_p = 2.84 \times 10^{-12} \sqrt{\frac{RT}{\rho_{liq} d_p^3}} \tag{24}$$

(It is more convenient to use c.g.s. units in equation (25) and to convert to feet per second by dividing by 30.48 cm/ft)

(9) Calculate N_{tot} from

$$N_{tot} = 18.08 \, \xi_p n_0 \tag{20}$$

(10) Calculate the deposition rate r from

$$r = N_{tot}\left(\frac{1}{6} \pi d_p^3\right) \tag{30}$$

where r is given in feet per second if N_{tot} is stated as particles per square foot second and d_p is given in feet.

An example of the calculation of boric oxide deposition on a typical turbine stator blade is shown in appendix B.

DISCUSSION AND APPLICATION OF RESULTS

Deposition Tests

The results of the deposition tests indicate that the preceding calculation method may be used to calculate boric oxide deposition rates on engine surfaces where conventional turbulent flow patterns exist (turbine stator blades and annular walls, tailpipes, exhaust nozzles, and ramjet engine combustors). The analysis is not valid in some regions that exist in jet engines: for example, surfaces where flow separation occurs, and surfaces on which a film of clean air is introduced (through pores or louvers). On surfaces where flow separation occurs, the deposition rate has been observed to be considerably less than on surfaces where uniform flow is present (see fig. 8 and discussion in previous section). The data of reference 8 indicate that deposits are greatly reduced on surfaces where air filming is employed (in ref. 8, a turbojet combustor), making calculation of deposition rates on these surfaces unnecessary.

The deposition rate alone, however, does not indicate completely the problem caused by the presence of liquid combustion products. If deposition occurred (with no run-off) at the rate of 4×10^{-4} inches per second (a typical figure for a pentaborane-fueled turbojet engine), a thickness of 1.44 inches would be present on the engine surfaces at the end of 1 hour of operation. In actual practice, deposits do not become this thick. The liquid oxide flows along surfaces because of the shear stress exerted on it by the flowing gas stream. At points where abrupt changes in surface profile occur, the flowing liquid film is sheared from the surface into the gas stream. After a period of time, the deposition rate equals the run-off rate; an equilibrium condition is then reached, and the film thickness will be a constant (as long as operating conditions remain constant). Although no data are presently available on the equilibrium film thickness, it is logical to assume that the thickness would be a function of either the shear stress acting on the liquid film or the kinetic force acting on waves formed in the film, similar to one of the following models:

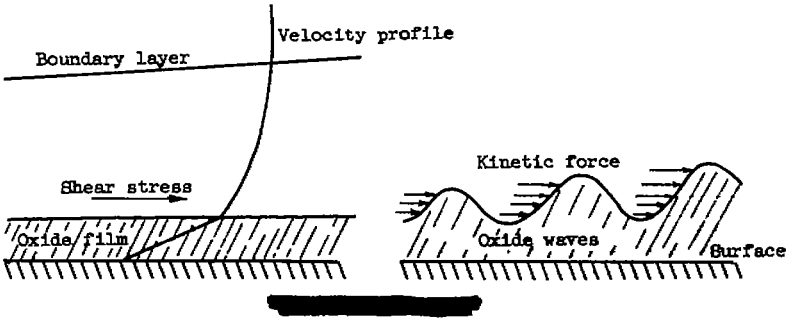

[redacted]

At the equilibrium condition (where the run-off rate is equal to the deposition rate), the deposition rate is important because it can be used in determining the amount of oxide running off turbine stators or being thrown from the tip of turbine rotors by centrifugal force.

Turbojet Engine Performance

Boron hydride fuels apparently show the greatest advantage in the primary combustor of the turbojet engine. Unfortunately, this application comprises the major problems arising from boric oxide deposition, and these difficulties occur mainly with the turbine (refs. 1 and 2). Shifts in turbine performance (which in turn can cause a fall-off in over-all engine performance) are shown in at least four ways:

(1) Formation of deposits on turbine stator blades reduces the flow area and thus requires an increased turbine-inlet pressure to maintain constant engine mass flow. The increase in turbine-inlet pressure (or compressor-discharge pressure) necessitates an increase in turbine work at constant mass flow.

(2) Any increase in turbine pressure ratio (increased turbine-inlet pressure or decreased turbine-discharge pressure) at constant engine mass flow results in a closer approach to the condition of limiting loading of the turbine rotor blades. As this condition is approached, the turbine-discharge Mach number increases, which results in high tailpipe total-pressure losses (accentuated by boric oxide deposits on tailpipe surfaces) and shock losses downstream of the throat section of the rotor blade.

(3) The presence of boric oxide deposits on turbine surfaces reduces the aerodynamic efficiency of the turbine because of increased friction losses.

(4) Changes in turbine operating conditions (such as increased pressure ratio) can cause losses in other engine components. For example, a higher turbine-discharge Mach number M_{td} can increase the tailpipe total-pressure loss due to friction (this friction loss is proportional to M_{td}^2). The effect of these losses on the performance of an actual engine is illustrated in the following discussion.

In the full-scale engine test of reference 1, a J65 engine (2-stage turbine) was run on pentaborane for 11 minutes. The engine was warmed up on 62-octane gasoline and it showed a specific fuel consumption (sfc, pounds of fuel per pound of net thrust per hour) of 1.365. Immediately after introduction of the pentaborane, the specific fuel consumption dropped to 0.942 (an improvement of 31 percent) but increased with run time until, at the end of the test (11 min), a value of 1.240 was reached.

However, since engine conditions did not remain constant during the run, the specific fuel consumption after 11 minutes of operation cannot be compared directly with that of gasoline at the beginning of the test.

This decay in engine performance was due mainly to an increase in tailpipe total-pressure loss which was caused by an increase in the turbine-discharge Mach number. This increase in turbine-discharge Mach number could have been caused by one or both of the following mechanisms:

(1) During the test, the turbine-stator area was calculated to have decreased about 5 percent (from 0.757 to 0.720 sq ft) because of boric oxide deposits. Consequently, to maintain constant engine mass flow, the turbine-inlet pressure had to be increased; this required an increase in compressor work and a corresponding increase in turbine work (which increases the turbine pressure ratio). The net effect was an increase in turbine-discharge Mach number M_{td}, which increased the friction pressure drop in the upstream portion of the tailpipe (this loss is proportional to M_{td}^2).

(2) After the test was completed, a buildup of boric oxide was observed near the trailing edge of the suction side of the second-stage stator blades. This buildup is attributed to flow separation that probably occurs near the trailing edge of these blades. The force of the gas stream acting on the oxide film on the forward part of the blade pushes oxide into the separation zone, where there is very little force present to remove it. This buildup of oxide pushes the point of flow separation upstream along the blade. The effect is a decrease in the tangential velocity vector at the stator exit, which requires a greater pressure ratio for the same turbine work output. To keep turbine work constant, the absolute velocity vector at the stator exit must be increased by increasing the turbine pressure ratio; this increases the turbine-exit Mach number (fig. 13).

This oxide buildup in zones of flow separation also occurred in the test section used during the tests reported herein. Figure 8(b) shows that a large accumulation of oxide occurred on the spacer-block surface just downstream of the wedge. Flow separation occurred at the intersection of the wedge and spacer block, and the oxide deposited on the wedge was pushed into the separated region, where the force on the oxide to produce further flow was very slight (fig. 14).

CONCLUDING REMARKS

Experimental data indicating that molecular diffusion across a thin layer is the controlling factor in the deposition of boric oxide are presented. A diffusion equation containing an experimentally determined constant is given, which enables the calculation of boric oxide deposit rates to within ±15 percent on surfaces where conventional flow patterns exist.

[redacted]

Knowledge of the behavior of liquid exhaust products is not complete. Additional work on run-off rates is required for the calculation of equilibrium thickness. Combined data on deposition rates and equilibrium thickness would greatly aid in the understanding of deposit patterns and subsequent engine performance losses. Such information also would be of value in alleviating the deposit problem.

Lewis Flight Propulsion Laboratory
National Advisory Committee for Aeronautics
Cleveland, Ohio, August 5, 1957

[redacted]

APPENDIX A

SYMBOLS

a	constant defined by eq. (5)
D	diffusion coefficient, sq ft/sec
d_p	particle diameter, cm or ft
g	acceleration due to gravity, 32.17 ft/sec^2
k	constant defined by eq. (5)
l	mean free path, ft
M	Mach number
m	molecular weight
N	particle flux due to diffusion, particles/(sq ft)(sec)
N_{Av}	Avogadro's number, 6.023×10^{23} molecules/mole
n	particle volume concentration, particles/cu ft
P	static pressure, atm
R	universal gas constant, units consistent with rest of equation
Re	Reynolds number, (xU_0/ν)
r	deposition rate, ft/sec
T	absolute temperature, $^\circ$R or $^\circ$K
t	time, sec
U	velocity, ft/sec
u	local velocity, ft/sec
v	volume, cu ft
W	weight, gm
X	number of lb-moles of gaseous combustion products/lb of B_2O_3

[redacted]

x,y,z	distance along coordinate axis, ft
Y	liquid volume concentration parameter, $Y = P/\rho_{liq}RT$
δ	full boundary-layer thickness, ft
δ_D	effective diffusion boundary-layer thickness, ft
η	defined by eq. (3)
ν	kinematic viscosity, sq ft/sec
ξ	molecular velocity, ft/sec or cm/sec
ρ	density, lb/cu ft
τ_w	wall shear stress, lb/sq ft
φ	equivalence ratio

Subscripts:

eff	effective
g	gaseous phase
liq	liquid phase
m	molecular
net	net
p	particle
T	turbulent
td	turbine discharge
tot	total
0	free-stream conditions

[redacted]

APPENDIX B

CALCULATION METHOD USED TO DETERMINE DEPOSITION RATE ON TYPICAL TURBINE STATOR BLADE

The stator-blade shape chosen for this calculation was taken from reference 10. The Mach-number distribution for this particular blade shape is shown in figure 15.

The calculation was made for the following conditions:

Fuel	Pentaborane
Equivalence ratio	0.2
Turbine-inlet static temperature, ^{o}R	2700
Turbine-inlet static pressure, atm	1.5
Combustor-exit Mach number (turbine inlet)	0.325
Ratio of specific heats	1.30
Stator-outlet mean Mach number	0.915
Stator Mach number distribution (from ref. 10)	Fig. 15
Particle diameter, cm	1.2×10^{-5}

The results of the calculation are summarized in table III and on figure 16.

REFERENCES

1. Breitwieser, Roland, and Useller, James W.: Performance of Pentaborane, Pentaborane - JP-4 Fuel Mixtures, and Trimethylborate Azeotrope Fuel in a Full-Scale Turbojet Engine. NACA RM E56G19, 1956.

2. Sivo, Joseph N.: Altitude Performance of a Turbojet Engine Using Pentaborane Fuel. NACA RM E57C20, 1957.

3. Thomas, C. A., and Eads, E. K.: Boric Oxide Deposition. Rep. CCC-1024-TR-15, Callery Chem. Co., Mar. 31, 1954.

4. Setze, Paul C.: A Study of Liquid Boric Oxide Particle Growth Rates in a Gas Stream from a Simulated Jet Engine Combustor. NACA E55I20a, 1957.

5. Streeter, Victor L.: Fluid Mechanics. McGraw-Hill Book Co., Inc., 1951.

6. Loeb, Leonard B.: The Kinetic Theory of Gases. Second ed., McGraw-Hill Book Co., Inc., 1934.

7. Schlichting, Hermann: Boundary Layer Theory. McGraw-Hill Book Co., Inc., 1955.

8. Kaufman, Warner B., Branstetter, J. Robert, and Lord, Albert M.: Experimental Investigation of Deposition by Boron-Containing Fuels in Turbojet Combustor. NACA RM E55L07, 1957.

9. Kaufman, Warner B., Lezberg, Erwin A., and Breitwieser, Roland: Preliminary Evaluation of Pentaborane in a 1/4-Sector of an Experimental Annular Combustor. NACA RM E56B13, 1957.

10. Hauser, Cavour H., and Nusbaum, William J.: Comparison of Results of Experimental and Theoretical Studies of Blade-Outlet Boundary-Layer Characteristics of Stator Blade for a High Subsonic Mach Number Turbine. NACA RM E56K29a, 1957.

TABLE I. - BOUNDARY-LAYER DATA

Run	Temperature, T, °R	Distance along axis, x, ft	Reynolds number, Re	Boundary-layer thickness, δ, ft	δ/x (a)	Run	Temperature, T, °R	Distance along axis, x, ft	Reynolds number, Re	Boundary-layer thickness, δ, ft	δ/x (a)
1	498	0.833	4.707×10^6	0.00451	0.00542	31	523	0.583	3.45×10^6	0.00328	0.00563
2	↓	↓	4.423	.00392	.00470	32	520	↓	3.288	.00333	.00571
3			3.405	.00372	.00447	33	515		3.018	.00305	.00523
4			2.381	.00458	.00550	34	505		3.726	.00290	.00497
5			5.272	.00400	.00480	35	505		2.55	.00300	.00514
6	701		1.493	.00516	.00620	36	504		1.72	.00543	.00931
7	745		2.076	.00512	.00615	37	531	.333	.150	.00327	.00982
8	750		2.521	.00425	.00510	38	↓	↓	.300	.00292	.00878
9	770		2.834	.00416	.00500	39			.532	.00223	.00699
10	773		3.232	.00425	.00510	40			.574	.00262	.00787
11	765		3.428	.00401	.00481	41	1591	.500	.8143	.00340	.00679
12	1249		1.441	.00541	.00650	42	1587	↓	.8157	.00352	.00703
13	1548		1.186	.00487	.00585	43	1546		.9953	.00350	.00701
14	1367		1.505	.00650	.00780	44	1607		1.0992	.00377	.00754
15	1560	↓	1.371	.00517	.00621	45	1618	↓	.9511	.00327	.00654
16	508	0.417	2.072×10^6	0.00215	.00515	46	791	0.500	0.09822×10^6	0.00530	0.01060
17	505	↓	1.112	.00301	.00723	47	763	↓	.1417	.00483	.00966
18	501		1.696	.00251	.00603	48	742		.1851	.00486	.00973
19	501		2.040	.00230	.00552	49	517	.833	.4709	.00526	.00632
20	500		2.959	.00218	.00524	50	↓	↓	.2679	.00724	.00869
21	498		2.882	.00205	.00493	51			1.165	.00501	.00602
22	706		1.631	.00245	.00588	52			.7204	.00584	.00701
23	700		1.498	.00251	.00601	53			.5399	.00800	.00961
24	717		1.225	.00282	.00676	54	642		1.911	.00419	.00503
25	720		.859	.00296	.00711	55	↓		1.595	.00499	.00599
26	1210		.218	.00425	.01020	56			1.321	.00518	.00622
27	1416		.298	.00341	.00818	57			.7871	.00583	.00700
28	1349		.281	.00355	.00852	58			.5446	.00636	.00763
29	1346		.251	.00375	.00900	59			.4519	.00659	.00791
30	556	↓	1.75	.00382	.00917		↓	↓			

[a] δ/x, ratio of boundary-layer thickness to distance from leading edge.

TABLE II. - SUMMARY OF DEPOSITION TESTS

Run	Fuel	Temperature, °R	Pressure, atm	Test section velocity, ft/sec	Particle concentration, particles/cu ft	Measured deposition rate, particles/sq ft-sec	Mean free path of particles, ft	Average velocity of particles, ft/sec	Theoretical molecular-diffusion coefficient, sq ft/sec	Effective diffusion coefficient, sq ft/sec
1	[a]TMB	1912	1.41	901	4.22×10^{13}	2.54×10^{14}	1.87×10^{-15}	3.58×10^{-1}	2.23×10^{-15}	1.13×10^{-14}
2		1878	1.11	758	3.62	2.48	2.56	3.68	3.14	1.75
3		1740	1.38	813	4.05	1.98	1.84	3.48	2.13	0.899
4		1716	1.07	658	3.34	2.04	2.52	3.57	3.00	1.54
5		1631	1.36	855	4.58	2.50	2.23	3.73	2.78	1.22
6		1655	1.13	926	5.17	3.76	3.78	4.33	5.45	2.75
7		1560	1.37	746	4.11	2.49	2.04	3.58	2.43	1.24
8		1572	1.07	588	3.20	1.88	2.60	3.58	3.10	1.53
9		1410	1.46	685	4.07	2.48	1.90	3.52	2.23	1.16
10		1490	1.13	510	2.83	1.67	2.08	3.30	2.28	1.23
11		1360	1.17	461	2.74	1.61	1.95	3.21	2.09	1.13
12		1287	1.02	552	3.70	3.00	3.70	3.96	4.88	3.00
13		1320	1.02	658	4.43	3.75	4.54	4.34	6.56	3.84
14	[b]B_5H_9	1716	1.00	890	2.99×10^{13}	1.46×10^{14}	0.882×10^{-15}	2.21×10^{-1}	0.649×10^{-15}	0.432×10^{-14}
15		1884	1.04	1123	4.99	2.66	1.64	2.96	1.61	.870
16		1530	1.01	798	4.17	3.30	1.79	2.96	1.76	1.41
17		1749	1.01	1004	4.85	2.74	2.05	3.19	2.18	1.16
18		1841	1.02	984	4.33	1.94	1.45	2.78	1.34	0.652

[a]TMB, Trimethyl borate - methyl alcohol azeotrope.

[b]B_5H_9, Pentaborane.

TABLE III. - CALCULATION OF TURBINE STATIC BLADE DEPOSITION RATES

Station	Distance from leading edge, ft	Pound-moles of gaseous combustion products/lb of B_2O_3, X	Temperature, T, °R	Static pressure, p, atm	Liquid volume concentration parameter, Y	Ratio of liquid to gaseous phase volume, v_{liq}/v_g	Particle concentration, n_0, particles/cu ft	Particle velocity, ft/sec	Total particle flux due to diffusion, N_{tot}, particles/(sq ft/sec)	Deposition rate, ft/sec
				Suction surface						
1	0.01667	0.82	2615	1.31	0.84×10^{-5}	1.02×10^{-5}	3.18×10^{14}	0.771	4.43×10^{15}	1.42×10^{-4}
2	.03334		2557	1.20	.71	.866	2.54	.760	3.49	1.12
3	.05000		2412	.908	.47	.573	1.78	.737	2.37	.761
4	.06668		2332	.784	.439	.535	1.67	.723	2.19	.704
5	.08333		2321	.767	.424	.517	1.61	.721	2.10	.673
6	.1000		2352	.812	.453	.552	1.72	.729	2.26	.726
7	.1167		2376	.851	.466	.568	1.77	.731	2.34	.750
8	.1333		2412	.908	.47	.573	1.78	.737	2.37	.761
9	.1500		2431	.939	.519	.633	1.97	.740	2.64	.846
				Pressure surface						
1	0.01667	0.82	2711	1.51	0.75×10^{-5}	0.915×10^{-5}	2.85×10^{14}	0.783	4.04×10^{15}	1.29×10^{-4}
2	.03334		2716	1.52	.75	.915	2.85	.783	4.04	1.29
3	.05000		2711	1.51	.75	.915	2.85	.783	4.04	1.29
4	.06668		2695	1.48	.72	.878	2.74	.781	3.87	1.24
5	.08333		2670	1.43	.71	.866	2.70	.779	3.80	1.22
6	.1000		2637	1.36	.67	.817	2.54	.772	3.55	1.14
7	.1167		2596	1.26	.63	.768	2.39	.766	3.31	1.09
8	.1333		2524	1.13	.61	.744	2.32	.753	3.17	1.02
9	.1500		2459	.990	.45	.549	1.71	.743	2.30	.739
				Leading edge						
0	0	0.82	2700	1.50	0.72×10^{-5}	0.878×10^{-5}	2.74×10^{14}	0.781	3.87×10^{15}	1.24×10^{-4}

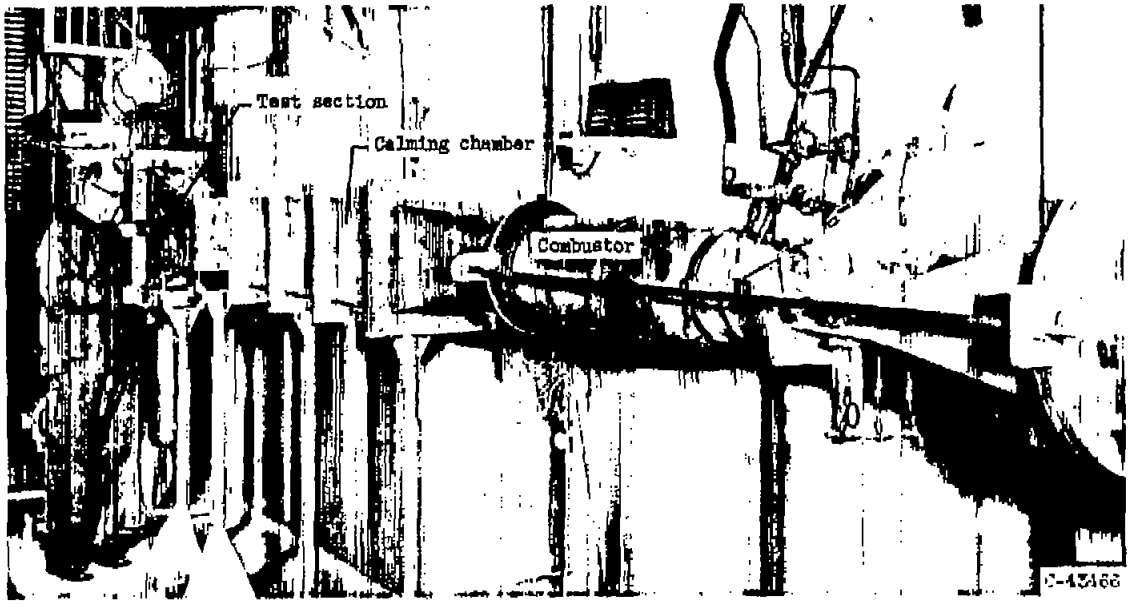

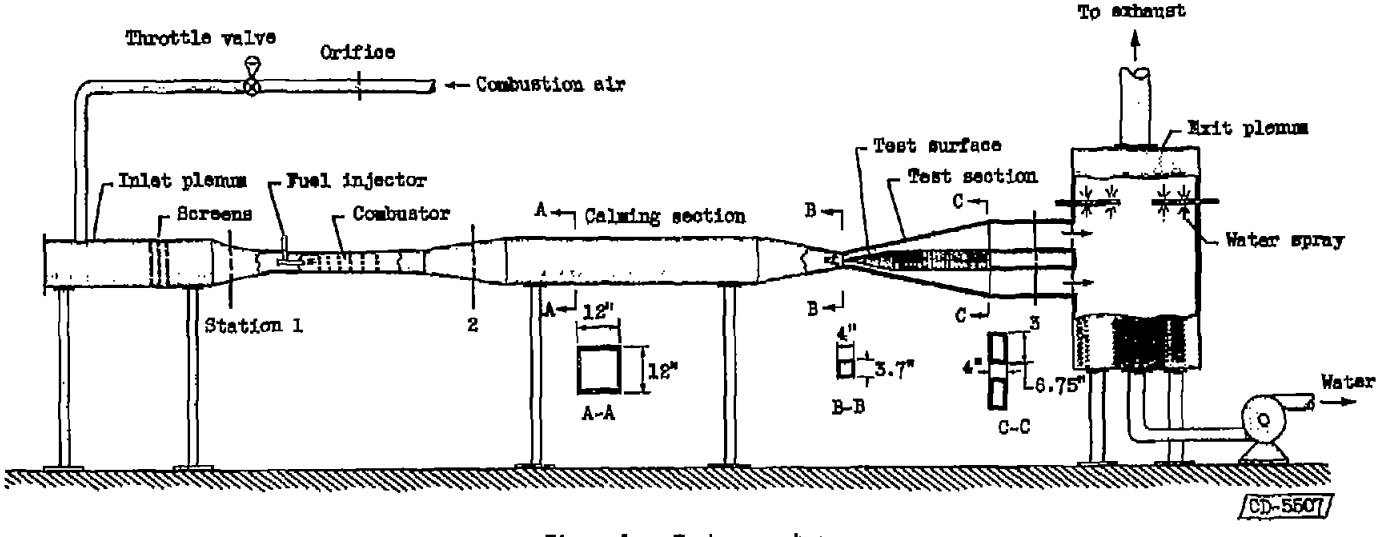

Figure 1. - Test apparatus.

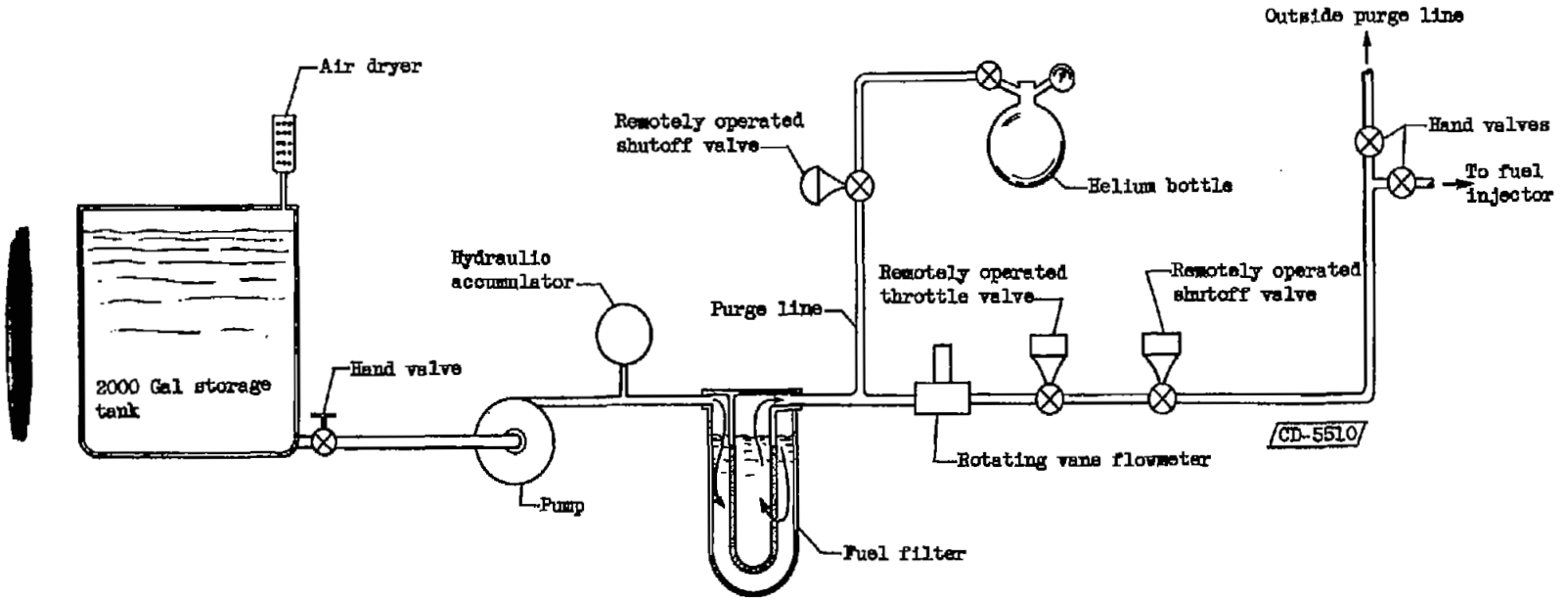

Figure 2. - Trimethyl borate fuel system.

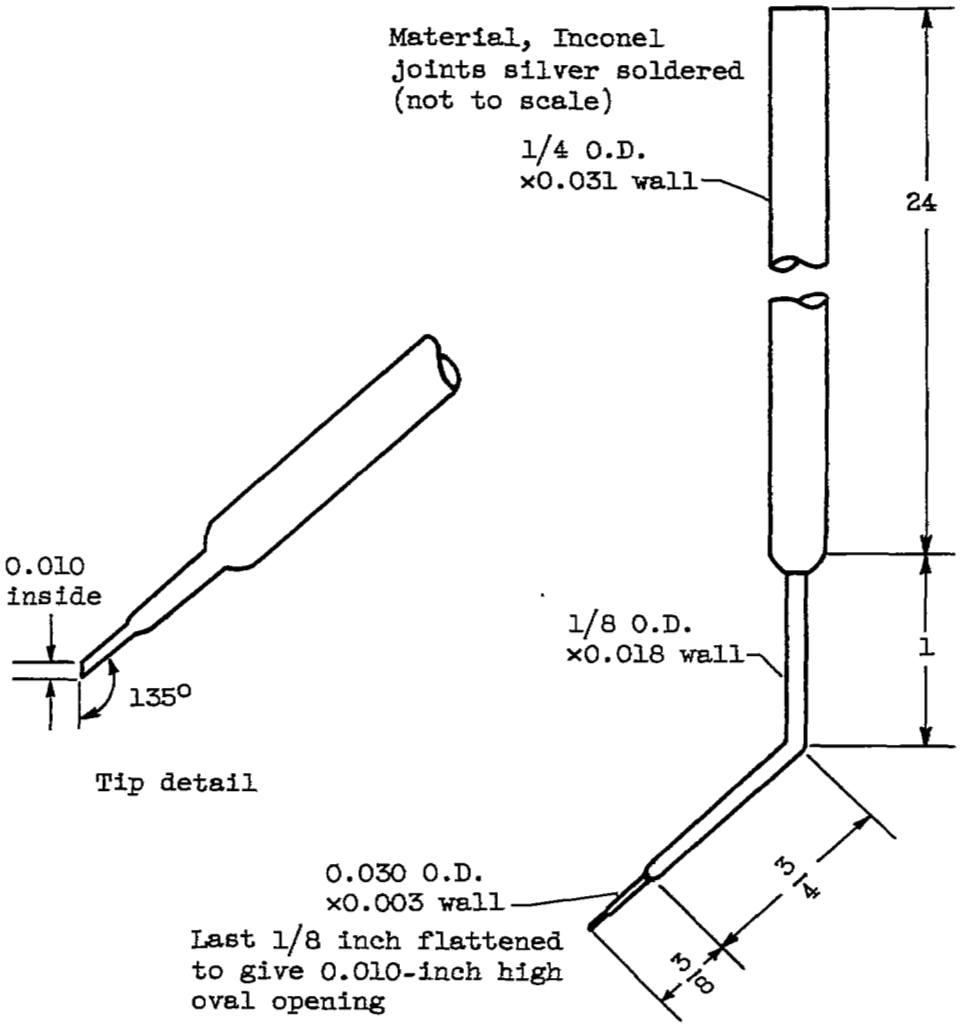

Figure 3. - Detail of total-pressure tube used in boundary-layer studies. (All dimensions are in inches.)

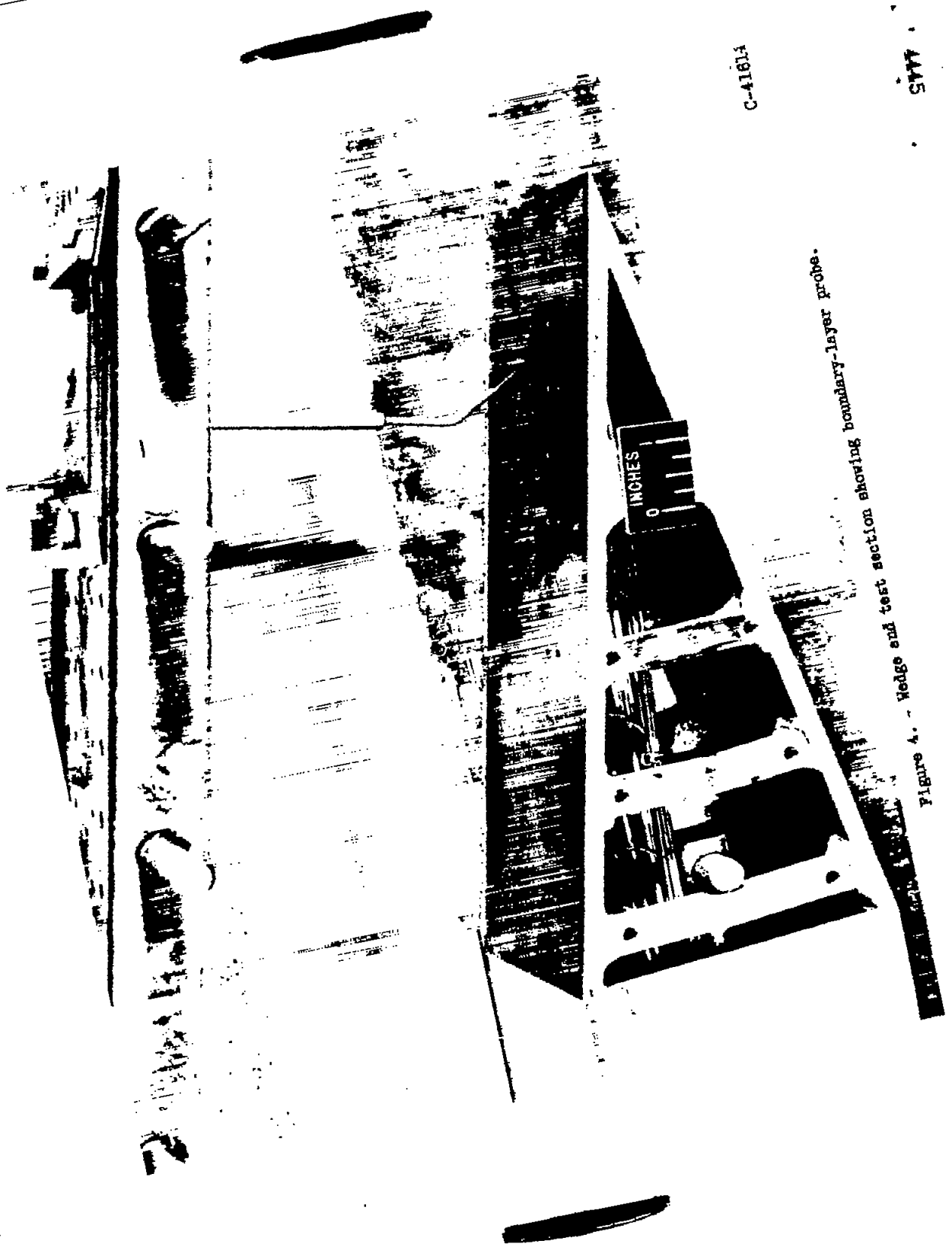

C-41614

4445

Figure 4. - Wedge and test section showing boundary-layer probe.

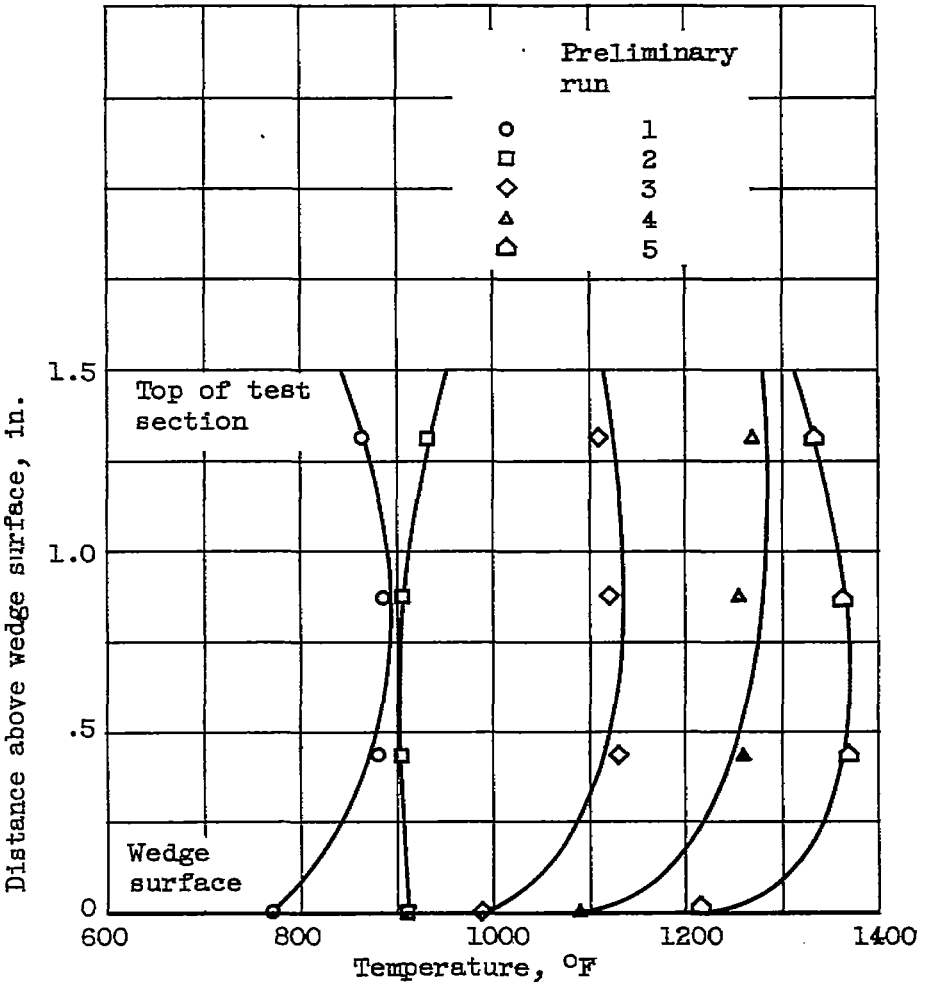

Figure 5. - Typical test-section temperature profiles.

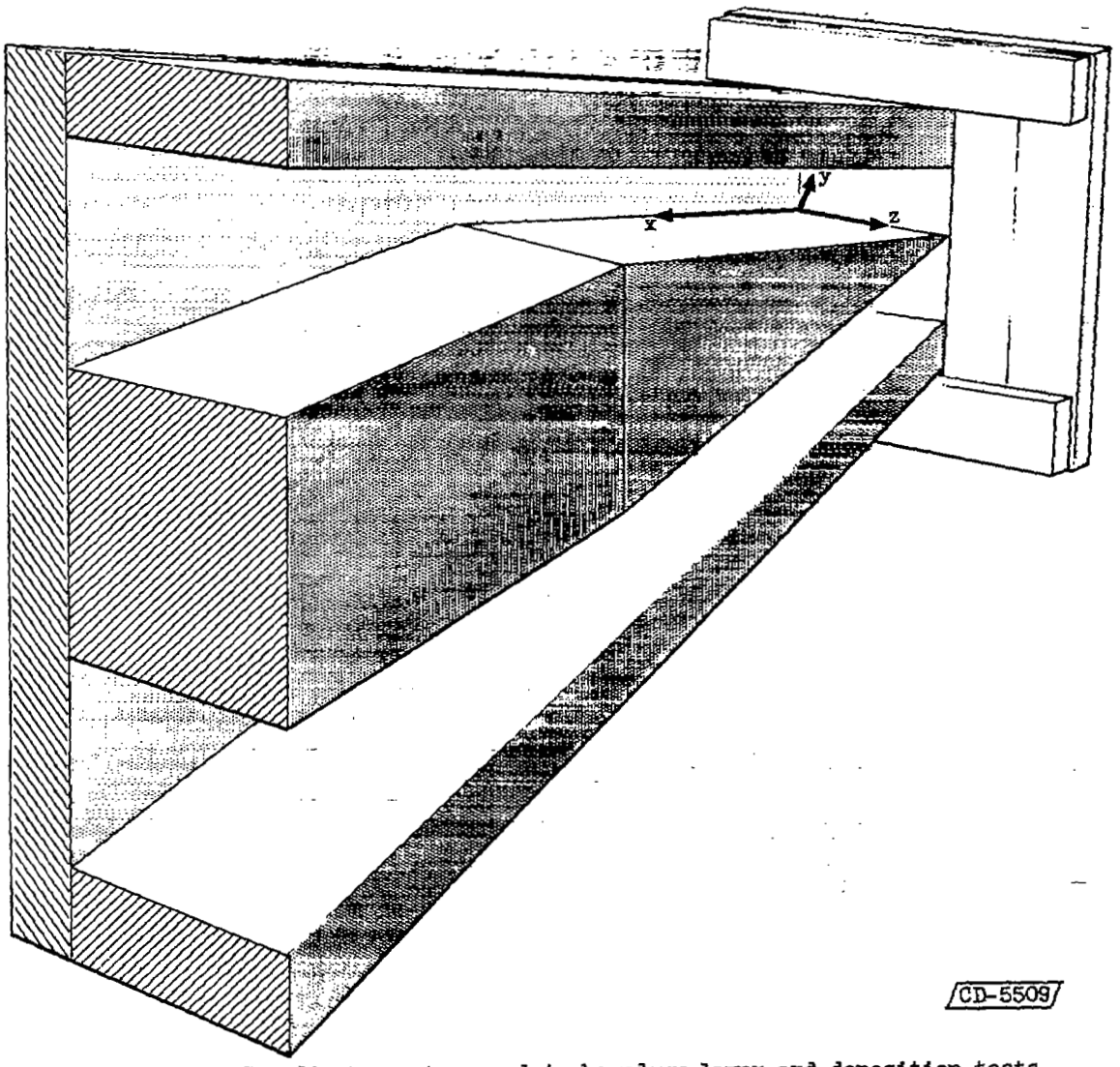

Figure 6. - Coordinate system used in boundary-layer and deposition tests.

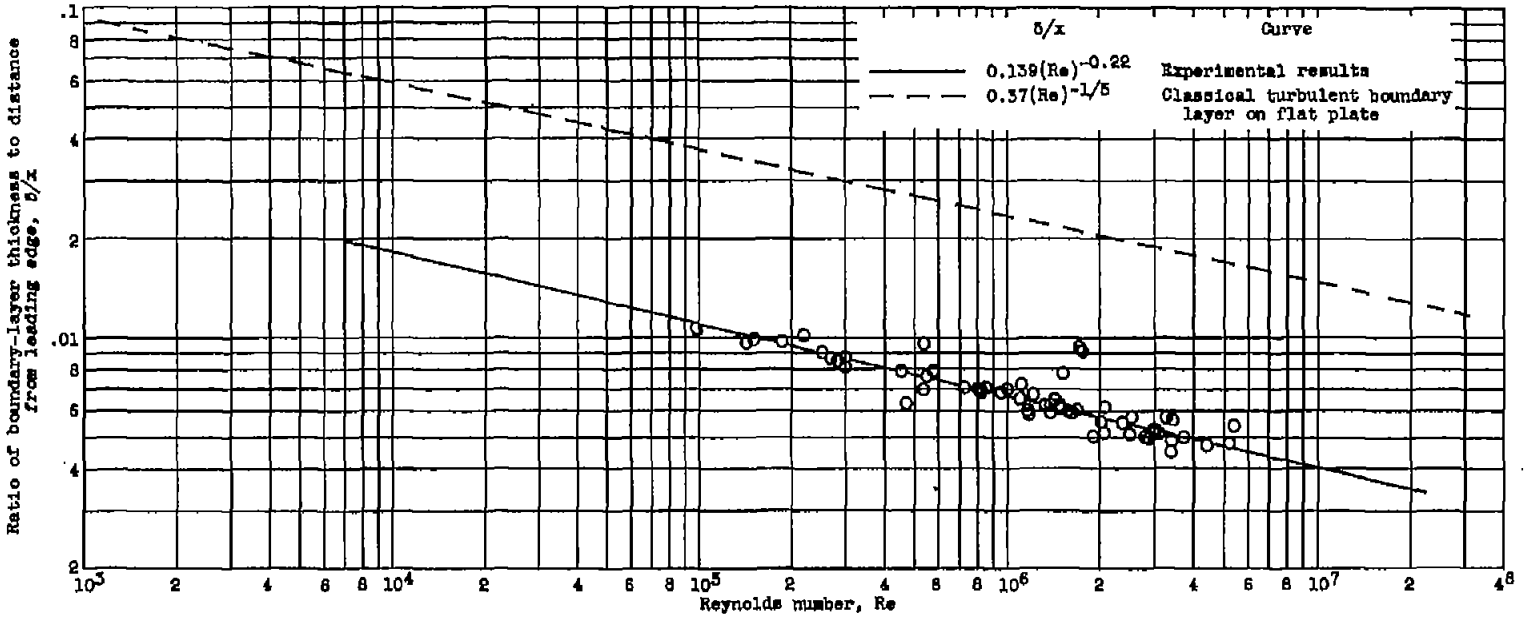

Figure 7. - Experimental results of boundary-layer study.

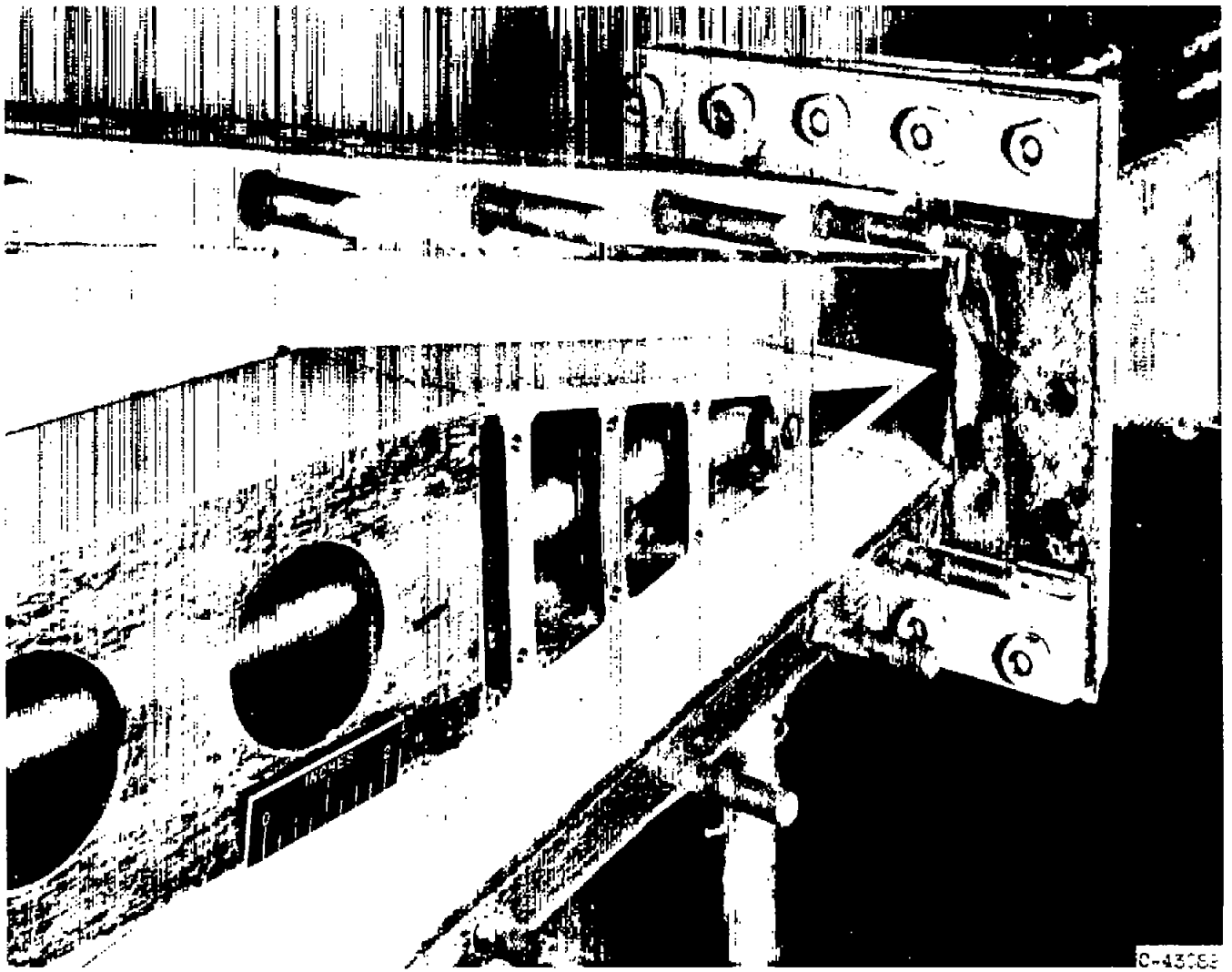

(a) A trimethyl borate fuel.

Figure 8. - Oxide deposits on wedge.

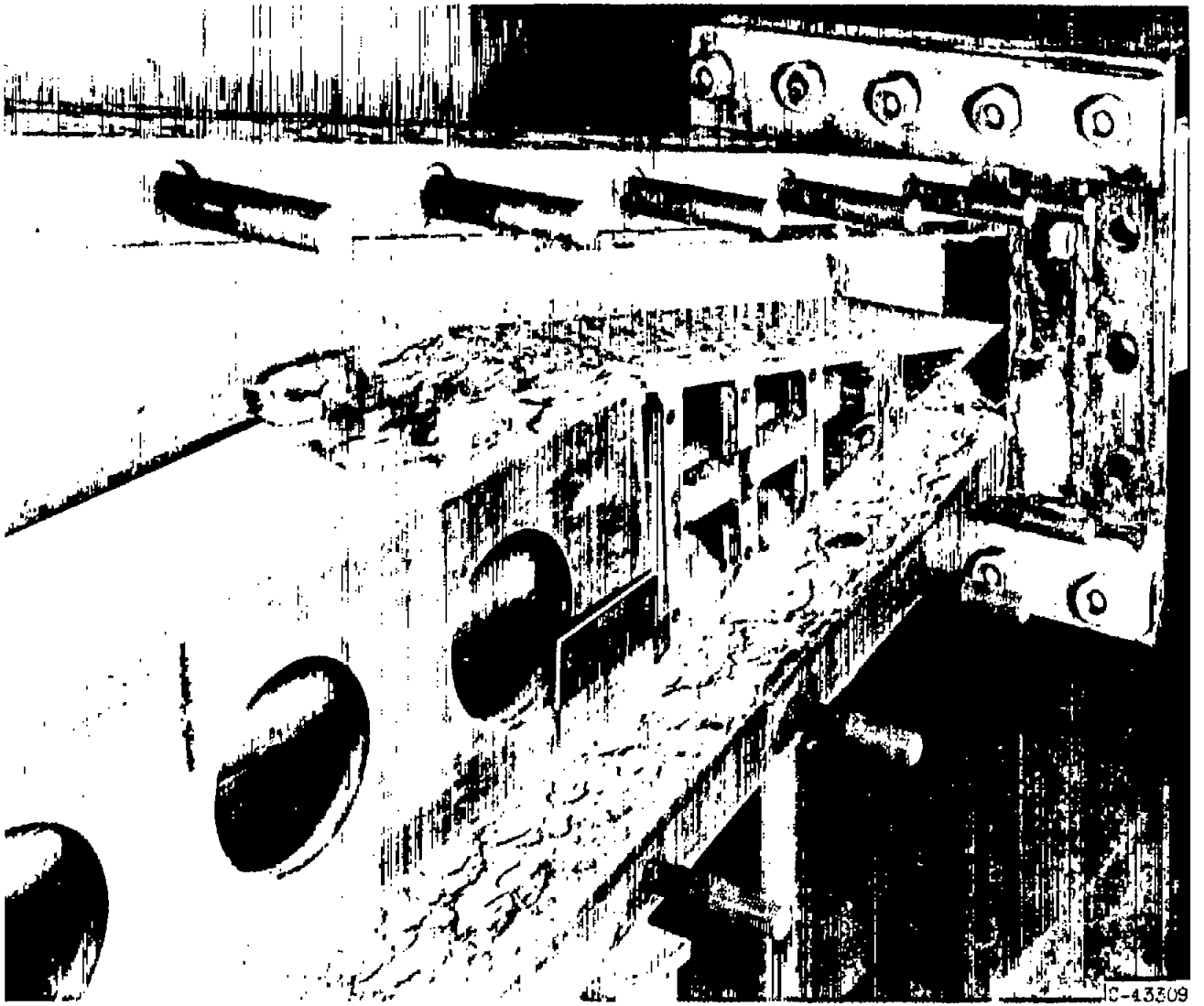

(b) Pentaborane fuel.

Figure 8. - Concluded. Oxide deposits on wedge.

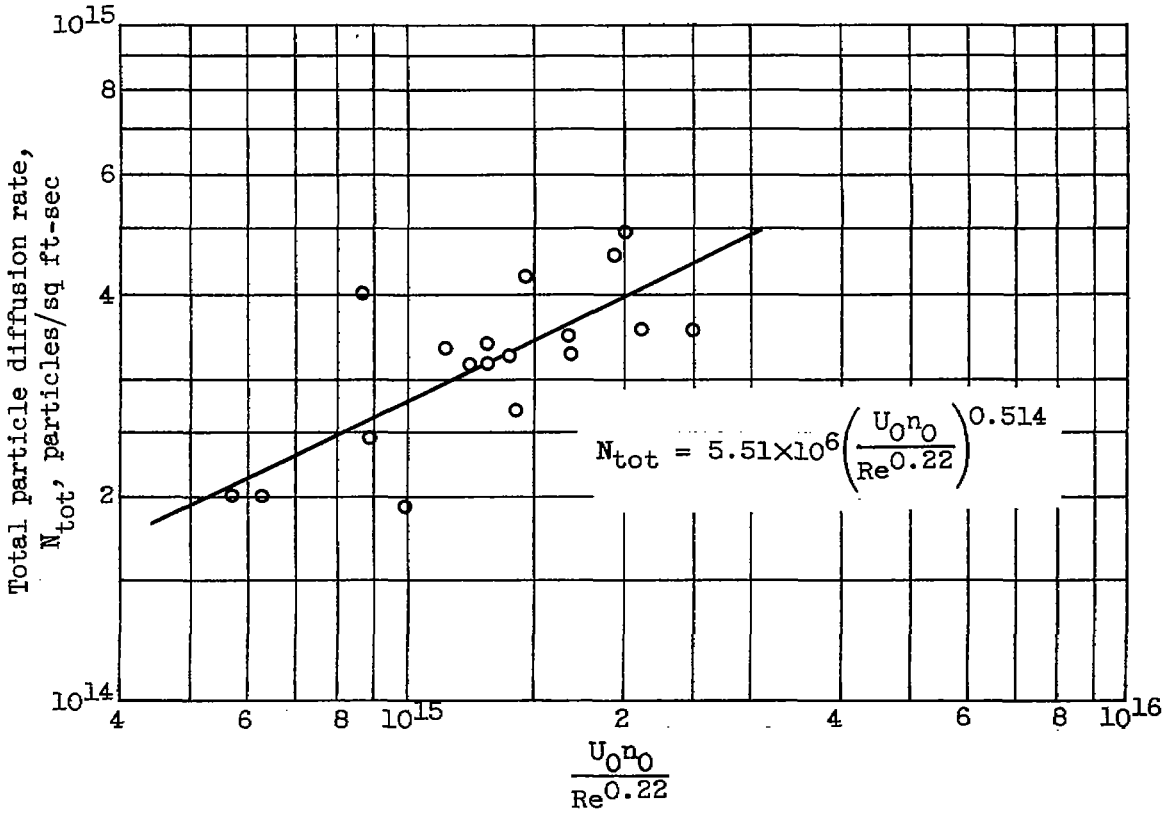

Figure 9. - Preliminary correlation of deposition data.

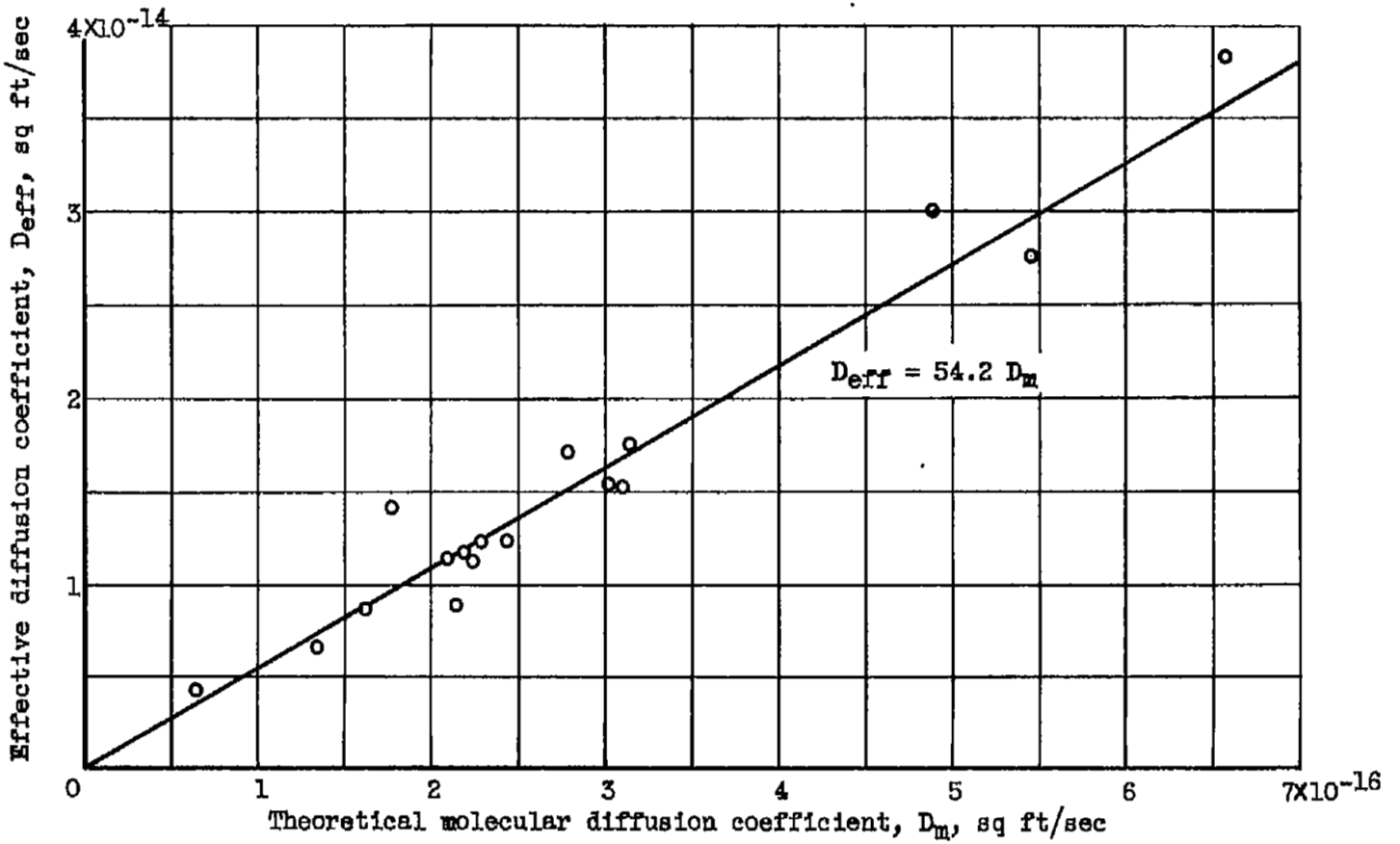

Figure 10. - Comparison of experimentally determined diffusion coefficient with theory.

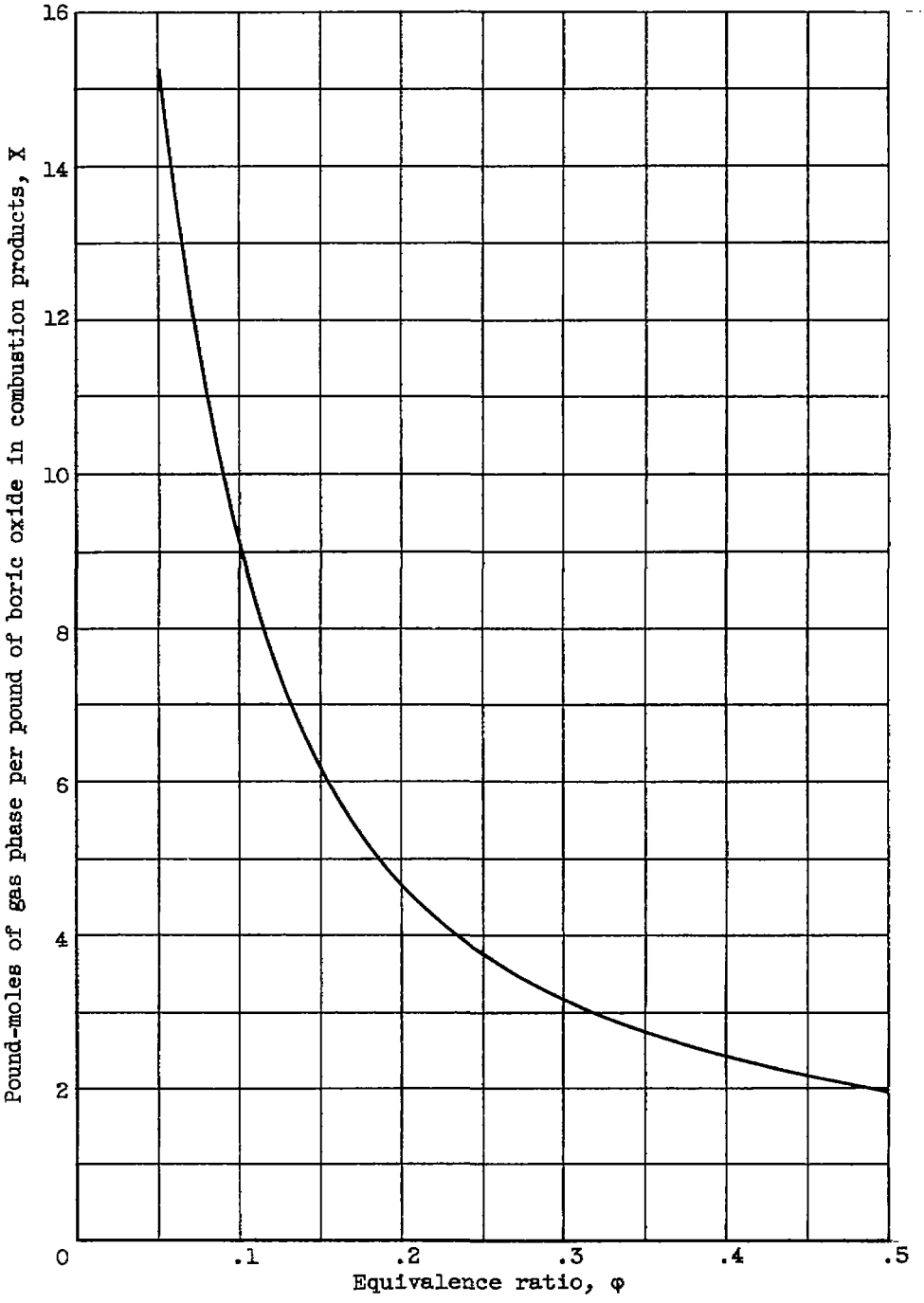

(a) Trimethyl borate - methyl alcohol azeotrope fuel.

Figure 11. - Pound-moles of gas phase per pound of boric oxide in combustion products plotted against equivalence ratio.

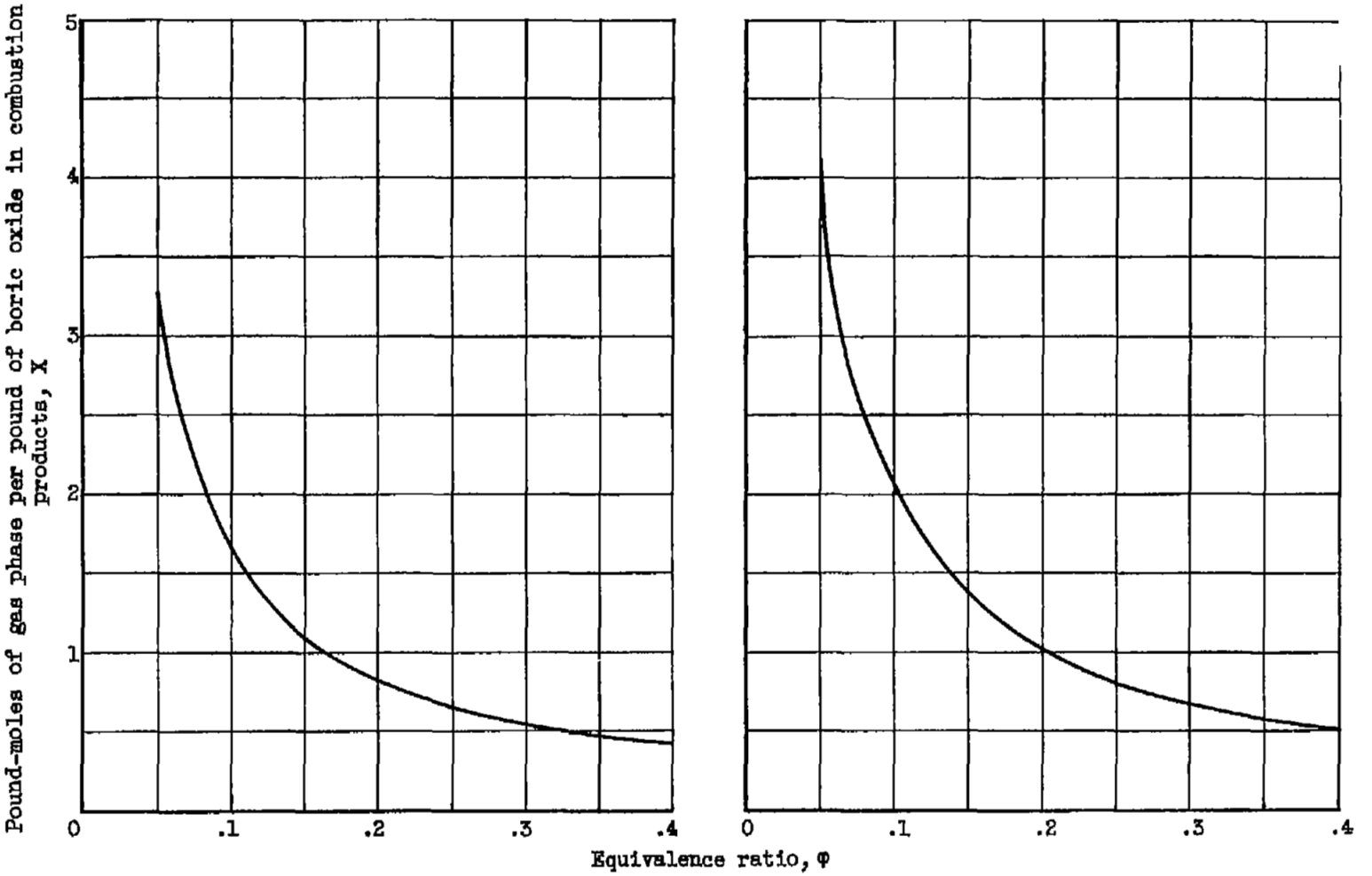

(b) Pentaborane fuel.

(c) Diborane fuel.

Figure 11. - Continued. Pound-moles of gas phase per pound of boric oxide in combustion products plotted against equivalence ratio.

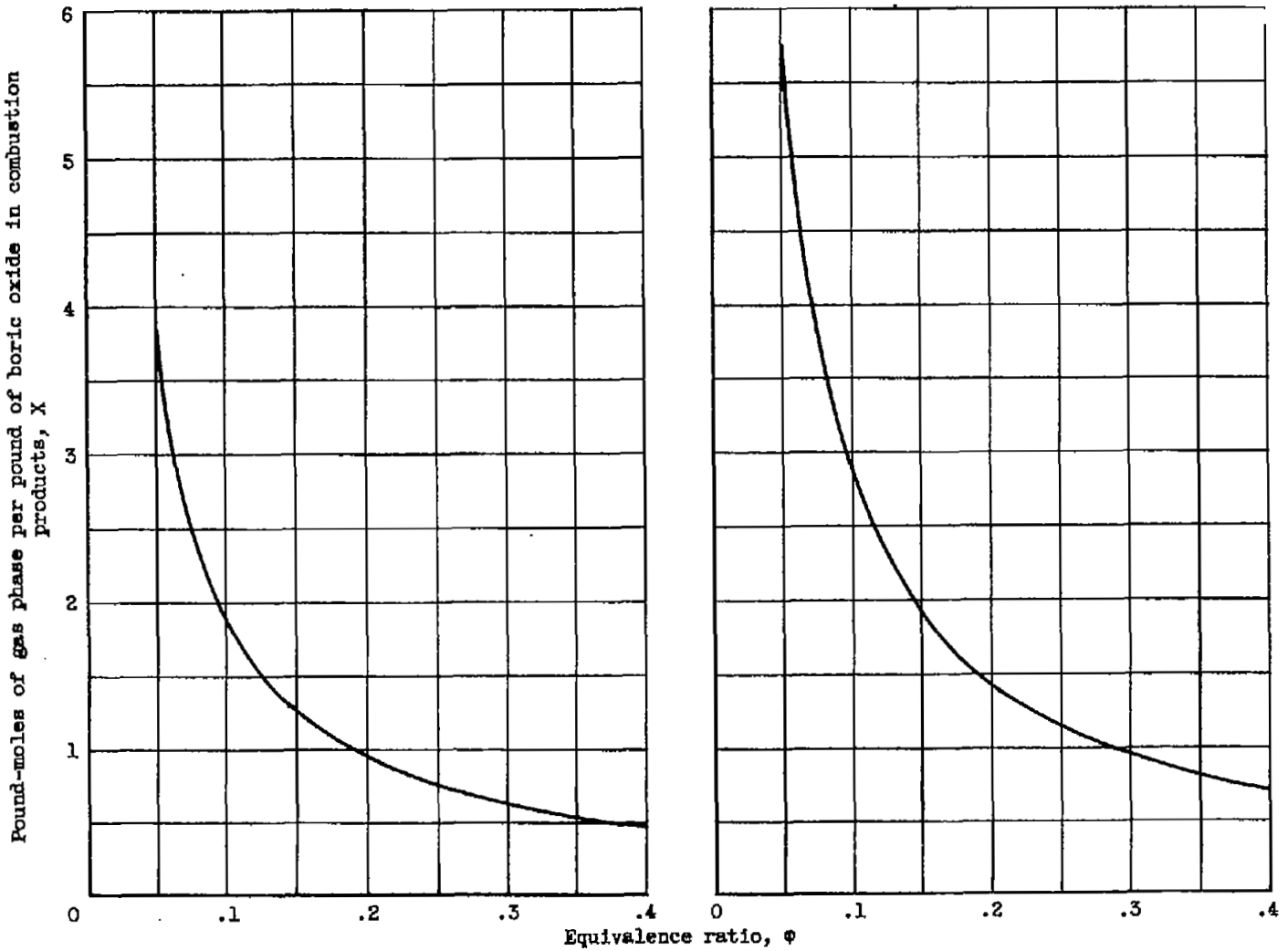

(d) Ethyl decaborane fuel.

(e) Propyl pentaborane fuel.

Figure 11. - Concluded. Pound-moles of gas phase per pound of boric oxide in combustion products plotted against equivalence ratio.

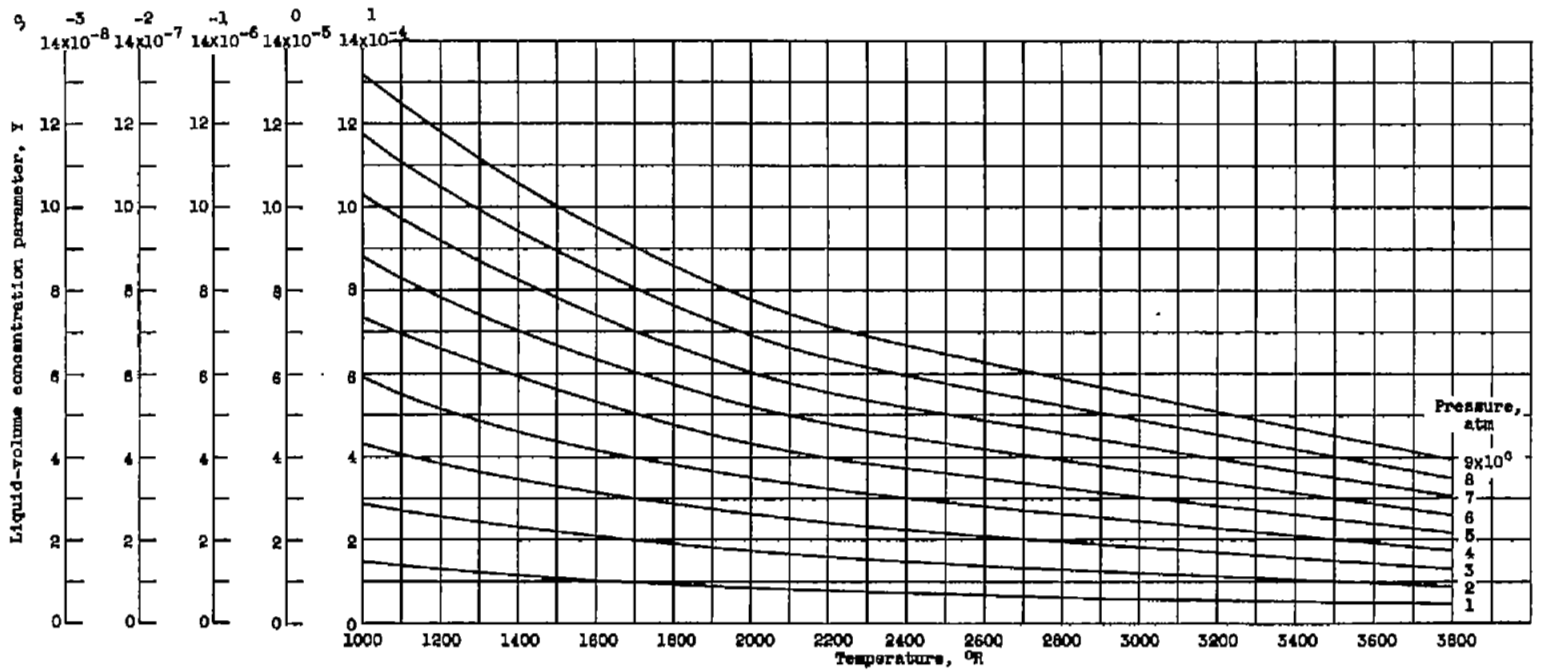

Figure 12. - Baric oxide liquid-volume concentration parameter as function of temperature and pressure.

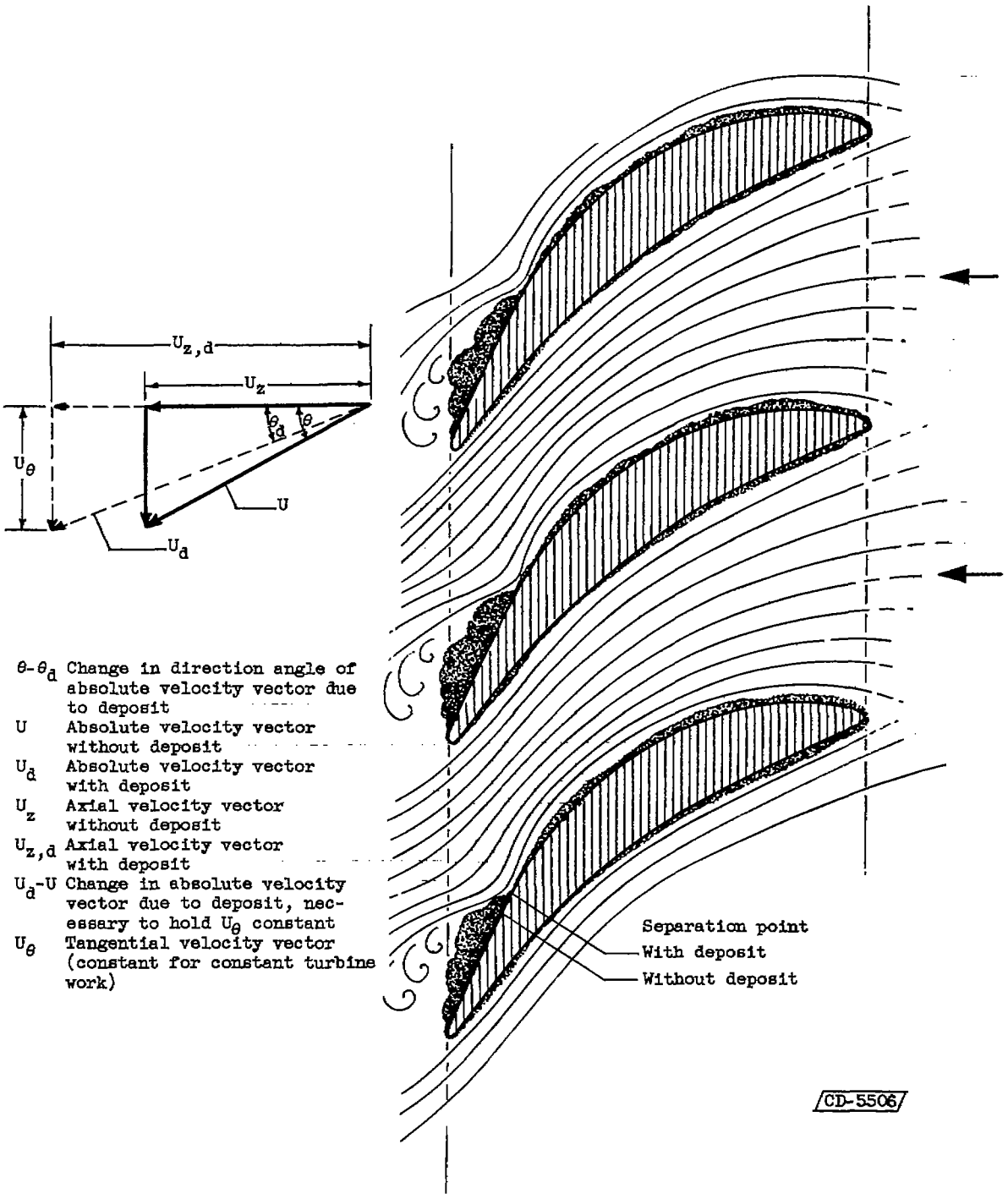

Figure 13. - Effect of flow separation on boric oxide buildup on trailing edge of turbine stator blades, with resulting effect on absolute velocity vector.

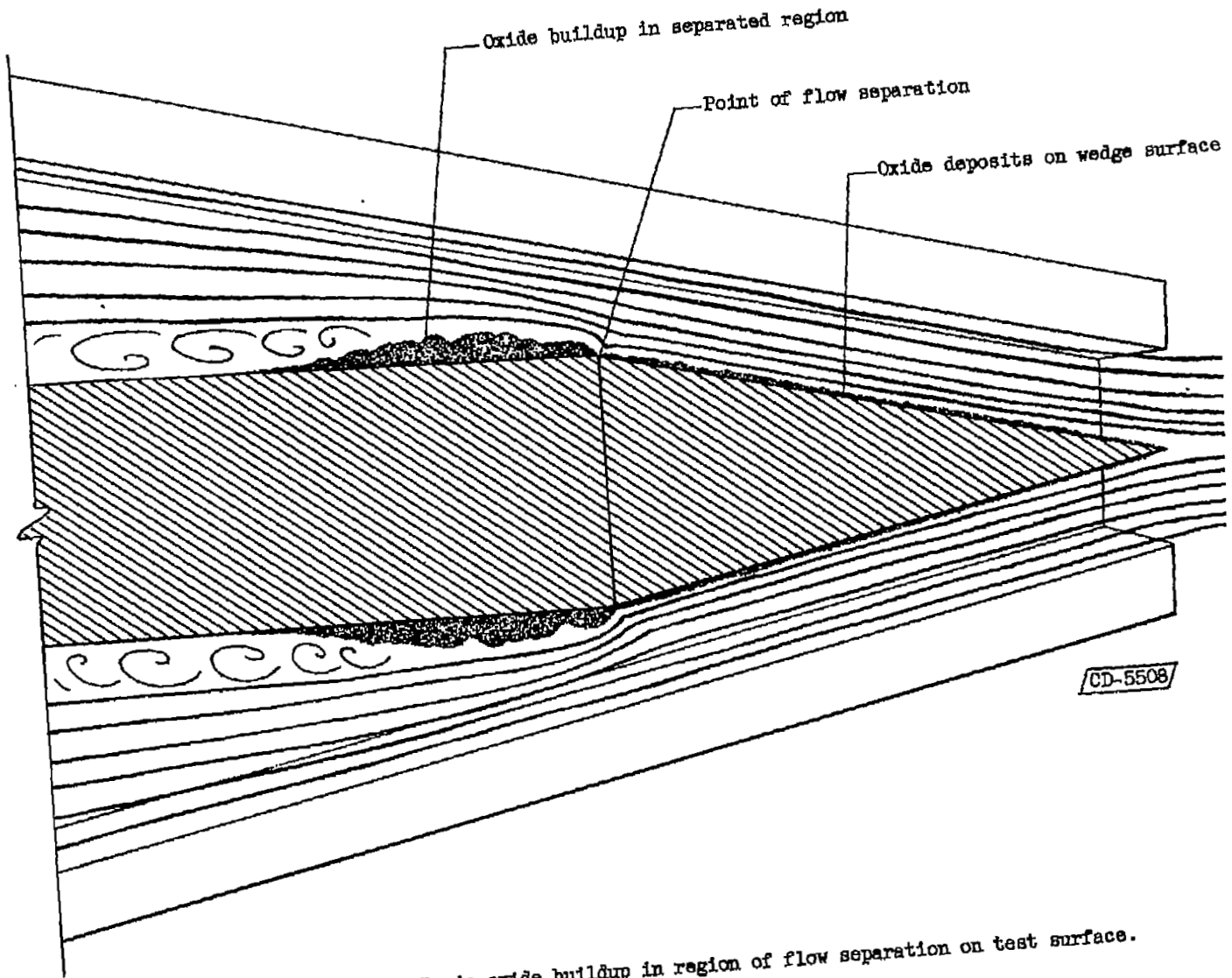

Figure 14. - Boric oxide buildup in region of flow separation on test surface.

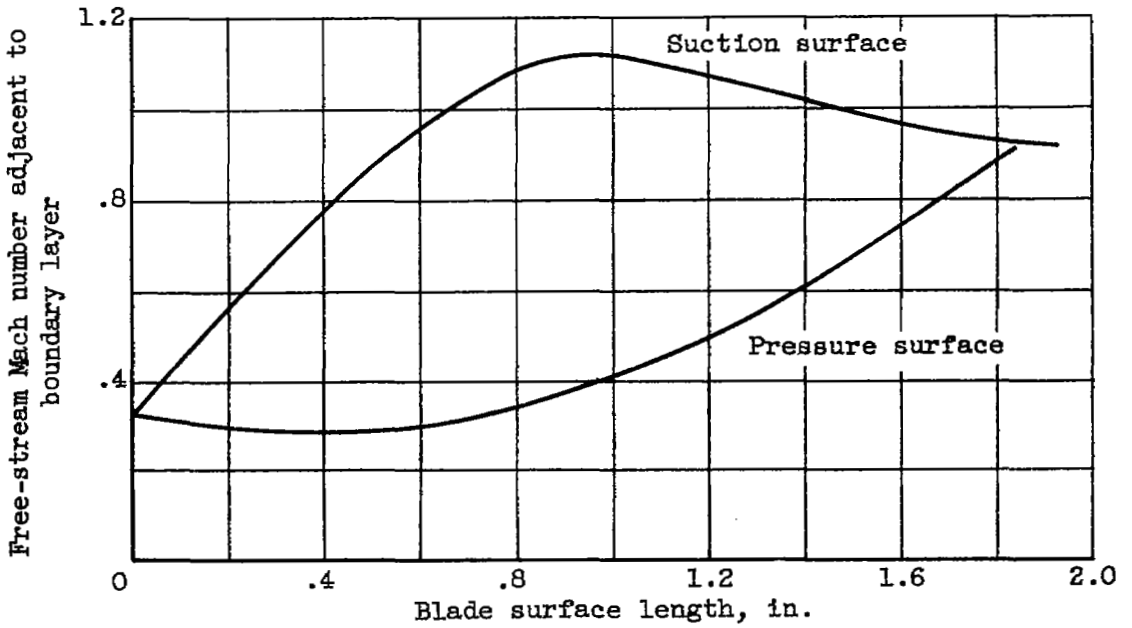

Figure 15. - Stator Mach number distribution. Exit Mach number, 0.915.

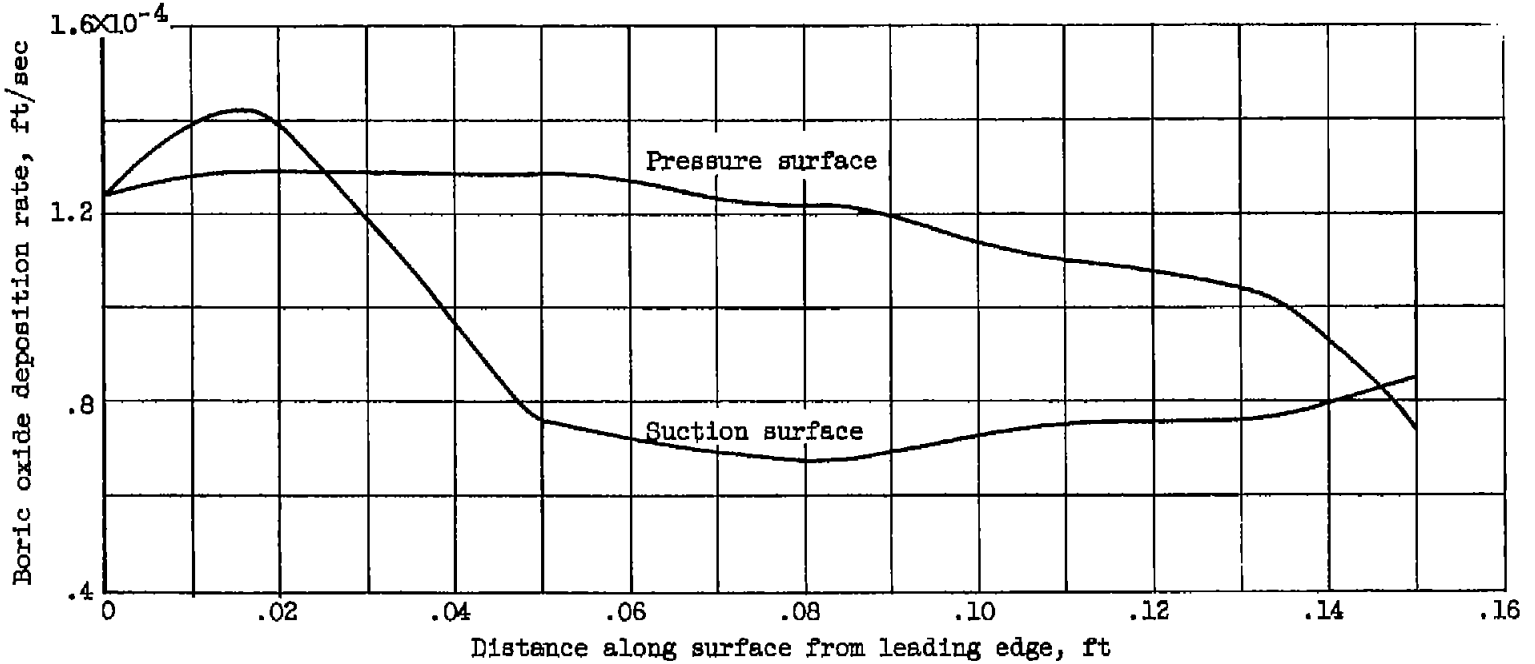

Figure 16. - Boric oxide deposition rate on turbine stator described in reference 10.